

Synergistic effects of previous winter NAO and ENSO on the spring dust activities in North China

Falei Xu¹, Shuang Wang¹, Yan Li², and Juan Feng¹

¹State Key Laboratory of Remote Sensing Science, Faculty of Geographical Science, Beijing Normal University, Beijing, China

²Key Laboratory for Semi-Arid Climate Change of the Ministry of Education, College of Atmospheric Sciences, Lanzhou University, Lanzhou, China

Correspondence: Juan Feng (fengjuan@bnu.edu.cn)

Abstract

Dust plays an important role in influencing global weather and climate ~~viably~~ impacting the Earth's radiative balance. Based on the ~~atmospheric and oceanic reanalysis~~ datasets during ~~1980~~1979-2022, the impacts of preceding winter North Atlantic Oscillation (NAO) and El Niño-Southern Oscillation (ENSO) on the following spring dust activities over North China are explored. It is found that both ~~the~~ NAO and ENSO exert significant effects ~~in influencing the on~~ dust activities ~~over in~~ North China, ~~particularly especially~~ during their negative phases. ~~A synergistic influence on the dust activities in North China is observed when~~ When both ~~NAO and ENSO~~of them are in ~~the~~ negative ~~phase,~~ ~~with phases,~~ their combined impacts ~~on the dust activities~~ exceeding that of either factor ~~alone individually~~. The previous winter NAO exhibits significant impacts on the sea surface temperatures (SST) in the North Atlantic, ~~associating associated~~ with an anomalous SST tripole pattern. ~~Owing to the persistence of~~These SST, ~~these~~ anomalies can ~~extend into~~persist to the following spring ~~due to their inherent persistence~~, when anomalous atmospheric teleconnection wave trains would be induced, thereby influencing the dust activities in North China. ENSO, on the one hand, directly impacts dust activities in North China by modulating the circulation in the Western North Pacific (WNP). ~~Moreover~~Additionally, ENSO enhances the NAO's effect on the North Atlantic SST, explaining their synergistic effects on the dust activities over North China. This study ~~explains elucidates~~ the combined ~~role roles~~ of NAO and ENSO on the dust ~~weather activities~~ over North China, providing one season ahead signals for ~~the forecast of predicting~~ spring dust activities in North China.

1. Introduction

Dust, as one of the most significant natural aerosols in the atmosphere, is of great importance to the global radiative balance with its light-absorbing properties, exerting a crucial role in climate change (e.g., Lou et al., 2017; Li et al., 2022; Kok et al., 2023). Moreover, dust not only influences its source regions but also extends its impact across oceans via teleconnections driven by atmospheric circulation. This transboundary transport affects ocean-atmosphere interactions and has a profound impact on the Earth's climate system (Huang et al., 2015). Dust ~~weather~~activities, resulting from regional dust surges, poses a formidable threat to socio-economic development, natural ecological environment, as well as human health and safety (Zhao et al., 2020; Li et al., 2023). The Gobi Desert in East Asia, particularly the Mongolian Plateau and ~~North~~Northern China, is a major source of dust (Chen et al., 2023; Hu et al., 2023), contributing approximately 70% of Asia's total dust emissions (Zhang et al., 2003). Given that China is one of the countries ~~most~~ profoundly impacted by dust ~~disasters~~activities (Fan et al., 2018), exploring the variations in dust ~~disasters~~activities in China is of significant scientific and practical importance.

Besides the dust source regions over China (mainly Xinjiang and Inner Mongolia), North China also exhibited high dust content and significant dust interannual variability (Liu et al., 2004; Ji and Fan, 2019). Additionally, as a crucial center ~~for~~of politics, economy, and population, it is meaningful to investigate the variations of spring dust ~~weather~~activities over North China (30-40°N, 105-120°E) and explore the relevant physical mechanisms. Previous studies have revealed that the frequency of dust events in China exhibits strong interannual and interdecadal characteristics, with high frequency from the 1950s to 1970s, low frequency from the 1980s to 1990s, and a ~~remarkable~~notable increase after 2000 (Zhu et al., 2008; Ji and Fan, 2019). On interdecadal time scales, climate oscillations such as the Atlantic Multidecadal Oscillation (AMO), Pacific Decadal Oscillation (PDO), as well as Antarctic Oscillation (AAO) can influence the dust activities by affecting the climate background. For instance, the positive phase of PDO is favorable for ~~less~~reduced dust ~~weather~~activities by influencing the westerly belt, leading to weaker dust activities (uplift and deposition) in the Asian region (Gong et al., 2006). The AMO plays a role in affecting the global aridification process by altering the thermal properties between land and sea (Huang et al., 2017). Additionally, the AAO may substantially regulate dust ~~weather~~activities in China by affecting the frequency of dust in East Asia through the interaction of meridional circulations between the Northern and Southern Hemispheres (Ji and Fan, 2019).

On the interannual scale, a weaker East Asian Winter Monsoon (EAWM) is associated with

62 anomalous circulation over the Gobi and Taklamakan deserts ~~facilitate, facilitating the~~ transport of
63 dust, consequently increasing dust content in China (Lou et al., 2016). The variations of the sea ice
64 coverage in the Barents Sea can significantly influence the intensity and frequency of dust
65 ~~weatheractivities~~ in China by ~~influencingaffecting~~ cyclone generation and thermal instability in
66 North China (Fan et al., 2018). The North Atlantic Oscillation (NAO) ~~can~~ exert a substantial
67 influence on the spring dust ~~weatheractivities~~ in North China by modulating the zonal wave train
68 from the Atlantic to the Pacific at mid-latitudes in the Northern Hemisphere, as well as the sea level
69 pressure (SLP) gradient in the Tarim Basin in China (Zhao et al., 2013). On the synoptic scale, the
70 NAO exerts a vital influence on the emergence and evolution of dust ~~weatheractivities~~ in North
71 China, ~~via its impact on~~ by impacting the transport of transient wave flux and ~~modifications~~
72 ~~iamodifying~~ atmospheric circulation (Li et al., 2023). Beyond extratropical signals, tropical
73 variabilities, such as El Niño–Southern Oscillation (ENSO), also significantly modulated dust
74 activities in China by regulating variations in large-scale circulation, precipitation, and temperature
75 over East Asia (Yang et al., 2022), as well as in Saudi Arabia (Yu et al., 2015), Central Asia (Xi and
76 Sokolik, 2015), and North America (Achakulwisut et al., 2017).

77 From the aforementioned studies on the dust activities in China, it is ~~seenevident~~ that the NAO
78 and ENSO are two important factors, with a focus on their individual effects on the dust
79 ~~weatheractivities~~ in China. However, as ~~one of the most~~ significant climate variabilities in the
80 extratropical and tropical regions, respectively, the NAO and ENSO often co-occur and have
81 complex interactions (López-Parages et al., 2015). It is found that ENSO can influence the climate
82 near the North Atlantic through atmospheric forcing of the Pacific–North America teleconnection
83 (Wallace and Gutzler, 1981). During the early winter of El Niño events, strong convective anomalies
84 in the tropical Indian Ocean–Western Pacific (Abid et al., 2021) and the Gulf of Mexico–Caribbean
85 Sea (Ayarzagüena et al., 2018) can trigger Rossby wave trains reaching the North Atlantic, leading
86 to positive NAO signals, and vice versa. Furthermore, the stratosphere, serving as an energy
87 transmission channel, may also be an important pathway for ENSO to influence the NAO (Jiménez-
88 Esteve and Domeisen, 2018). Moreover, observations and numerical simulations have demonstrated
89 that the NAO signal can induce a Gill–Matsuno pattern in the tropical region of southern Eurasia,
90 inducing a decadal enhancement in the linkage between the East Asian Summer Monsoon (EASM)
91 and ENSO (Wu et al., 2012). When the NAO is in its positive phase, intensified northeasterlies are
92 observed over tropical North Atlantic, resulting in increased low-level moisture content and
93 precipitation in the tropical North Atlantic, paralleling with stronger convection and enhanced
94 ENSO impact (Ding et al., 2023). These ~~researchesstudies~~ highlight the connections and interactions

95 between NAO and ENSO, underscoring the necessity of considering their synergistic effects on the
96 dust activities in North China.

97 The synergistic effect refers to the phenomenon where the combined impacts of two or more
98 factors ~~is~~are significantly greater than their individual ~~roles~~roles (Li et al., 2019). It ~~is~~has been found
99 that there are synergistic effects in the impact of NAO and ENSO on the weather and climate ~~over~~in
100 China. The NAO can facilitate the development of the subpolar teleconnection across northern
101 Eurasia downstream, leading to anomalies in the high-pressure systems over the Ural Mountains
102 and the Sea of Okhotsk, which in turn affect the EASM (Wang et al., 2000). Meanwhile, ENSO
103 exerts significant impact on the convective activities in the central Pacific and induces alterations
104 in the equatorial circulation via the Pacific-East Asia teleconnection, further affecting the
105 atmospheric circulation and sea surface temperature (SST) in the Western North Pacific (WNP),
106 ultimately influencing the intensity of the EASM (Wang et al., 2000). Therefore, the synergistic
107 effects of these factors can result in pronounced impacts on the EASM (Wu et al., 2009). During El
108 Niño events, SST in the central and eastern equatorial Pacific rises, enhancing convective activity
109 near the equator, which brings more moisture to North China and increases the likelihood of
110 precipitation. Simultaneously, the positive phase of NAO can alter atmospheric pressure in the North
111 Atlantic, influencing atmospheric circulation over the Eurasian continent. This interaction between
112 NAO and ENSO synergistically regulates, to some extent, the distribution of precipitation in North
113 China (Guo et al., 2012).

114 ~~It is evident that the~~The synergistic effects of NAO and ENSO ~~exert significant impacts on~~
115 ~~significantly influence~~ the climate in China. ~~However, the, but their~~ synergistic ~~impacts of these two~~
116 ~~factor~~effects on the dust ~~events in activities over~~ North China ~~remains unclear,~~ and the ~~underlying~~
117 mechanisms ~~and processes are yet to be elucidated. Therefore, this~~involved remain unclear. This
118 study will ~~examine the synergistic~~investigate these effects of NAO and ENSO on the dust ~~weather~~
119 ~~in activities over~~ North China. ~~Moreover, given that the impacts of winter NAO and ENSO on the~~
120 ~~climate in China is more pronounced (Zuo et al., 2016; Zhang et al., 2021b), our analysis will~~
121 ~~concentrate on the influence of previous winter NAO and ENSO on the following spring dust,~~
122 ~~thereby,~~ providing a scientific foundation for predicting dust ~~events~~activities in China. The structure
123 of this paper is as follows: Section 2 outlines the datasets and methods employed in this study.
124 Section 3 presents the analysis and findings. Section 4 contains the summary and discussion.

125

126

2. Datasets and methods

2.1 Datasets

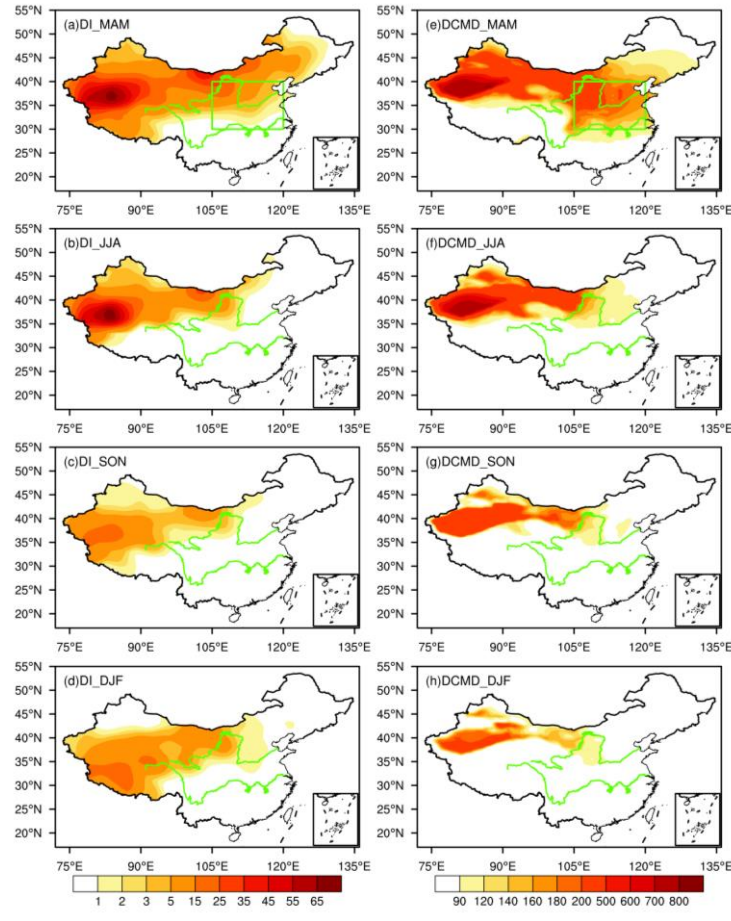
The dust dataset for the Modern-Era Retrospective Analysis for Research and Applications Version 2 (MERRA-2) was obtained from NASA's Global Modeling and Assimilation Office (GMAO), incorporating assimilated observations from both satellites and ground stations (Gelaro et al., 2017). In this study, the Dust Column Mass Density of the MERRA-2 `tavg1_2d_aer_Nx` product was utilized to represent the dust ~~concentration with $0.5^\circ \times 0.625^\circ$ resolution.~~ content with a $0.5^\circ \times 0.625^\circ$ resolution. Previous studies have demonstrated the applicability of MERRA-2 reanalysis data for simulating the spatiotemporal distribution characteristics of dust aerosol content in China (Kang et al., 2016; Wang et al., 2021). It is reported that the result based on MERRA-2 are similar to those obtained from MODIS, OMPS, CALIPSO, and Himawari-8 data (Kang et al., 2016; Wang et al., 2021). Additionally, we further employ the datasets from the China National Meteorological Centre from 1980-2018, which include observations of floating dust, blowing dust, and dust storms, to validate the reliability of MERRA-2 reanalysis data. The frequency of dust activities recorded at these stations has been converted into a Dust Index (DI) (Wang et al., 2008; Equations 1), effectively representing the content of dust aerosols.

$$DI = 9 \times DS + 3 \times BD + 1 \times FD \quad (1)$$

Where DS, BD, and FD represent the frequency of dust storms, blowing dust, and floating dust, respectively. Additionally, DI denotes the content of dust aerosols at each station. We found that the variations of the DI and MERRA-2 dust aerosols content during the four seasons all show similar spatial characteristics (Figure 1). Especially for the dust source in northwest China and the spring dust aerosols over North China, the spatial distribution characteristics are relatively consistent. The above results indicate that the MERRA-2 aerosol reanalysis data can capture the spatiotemporal characteristics of dust aerosol content in China, which is applicable for us to understand the variations in dust aerosol content in China.

Additionally, the SST dataset was derived from the Hadley Centre of the UK Met Office on a $1^\circ \times 1^\circ$ grid (Rayner et al., 2003). The atmospheric reanalysis datasets employed herein were provided from the Fifth Generation Reanalysis Version 5 (ERA5) of the European Centre for Medium-Range Weather Forecasts (ECMWF) with a resolution of $0.25^\circ \times 0.25^\circ$ on 37 vertical levels (Hersbach et al., 2020), including wind, geopotential height, and sea-level pressure, specific humidity, precipitation, and vorticity field. Considering the available period of all datasets, the

158 common available period of 1979–2022 was selected. The winter is defined as December-February
 159 (December-January-February, DJF), with the winter of 1979 corresponding to the average of
 160 December in 1979, January and February in 1980. ~~The spring season is delineated as~~ To focus the
 161 average of March–May (March–April–May, MAM)-investigation into the interannual variability, the
 162 linear trends of all variables were removed.



163
 164 **Figure 1.** (a-d) Spatial distribution of seasonal mean DI based on station data, (e-h) as in (a-d), but
 165 for dust column mass density based on MERRA-2 (units: $\text{mg}\cdot\text{m}^{-2}$). The green box in (a) and (e)
 166 represents North China. The green lines represent the Yellow River (northern one) and the Yangtze
 167 River (southern one), respectively.

168 2.2 Methods

169 The NAO index (NAOI) used is following Li and Wang (2003), quantified by the difference in
 170 the normalized monthly SLP regionally zonal averaged over the North Atlantic within 80°W-30°E
 171 between 35°N and 65°N. This definition effectively captures the large-scale circulation
 172 characteristics associated with NAO, essentially measuring the intensity of zonal winds spanning
 173 the entire North Atlantic. We also employed the NAOI produce by Hurrell (1995) and Jones (1997),
 174 which have been used in many studies (e.g., Wang et al., 2022; Najibi et al., 2023; Parry et al., 2023).

175 A good agreement with correlation coefficients of 0.96 and 0.94 between these two indices and the
176 NAOI defined by Li and Wang (2003). Furthermore, ENSO is characterized by Niño3.4 index with
177 SST anomalies averaged over 5°S-5°N, 170°W-120°W (Trenberth, 1997). In this study, we utilized
178 the standardized indices of seasonal averages during 1980-2022, with values exceeding 0.5 standard
179 deviations identified as anomalous years as shown in Table 1.

180 In this study, we utilized the standardized indices of seasonal averages during the previous
181 winter (the winter from 1979 to 2021), with values exceeding 0.5 standard deviations identified as
182 anomalous years, as shown in Table 1. The winter NAO and ENSO indices are during 1979-2021,
183 and the spring dust are during 1980-2022, to highlight the preceding impacts of previous winter on
184 the following spring. The correlation analysis is used to explore the relationship between
185 NAO/ENSO and dust content over North China, and the composite analysis is employed to
186 investigate the synergistic effects of these climatic variabilities on the dust activities over North
187 China. The statistical significance of the correlation, regression and composite values was evaluated
188 by a two-sided Student's *t*-test.

189 The memory effect of SST can be elucidated by the SST persistence component (SST_p), as
190 delineated in equation (2) (Pan, 2005).

$$191 \quad SST_p = SST(t) * \frac{Cov[SST(t), SST(t + 1)]}{Var[SST(t)]} \quad (2)$$

192 SST_p represents the memory effect of the previous SST (previous winter) on the following SST
193 (spring), where $SST(t)$ and $SST(t + 1)$ denote the previous winter SST and spring SST,
194 respectively. $Cov[SST(t), SST(t + 1)]$ denotes the covariance between the previous winter SST
195 and spring SST, while $Var[SST(t)]$ signifies the variance of the previous winter SST.
196 Consequently, the $Cov[SST(t), SST(t + 1)]/Var[SST(t)]$ represents the connection between the
197 SST variations in previous winter and spring. A greater value of SST_p indicates the variation of
198 $SST(t + 1)$ is more closely attached with the variation of $SST(t)$.

199 The T-N wave activity flux (WAF), formulated by Takaya and Nakamura (2001), represents a
200 three-dimensional wave action flux that describes the energy dispersion characteristics of stationary
201 Rossby waves, thereby reflecting the direction of Rossby wave energy dispersion. The WAF is
202 suitable for application in mid-high latitude regions where the background circulation deviates from
203 uniform zonality, as obviates the need for the assumption that the basic flow field must be a zonally
204 averaged basic flow and can accommodate zonally non-uniform wind fields. The convergence and
205 divergence characteristics of WAF reveal the source and dissipation areas of wave energy, with the
206 transmission direction being interpretable as the direction of energy transport. The three-

207 dimensional formulation of WAF is as follows:

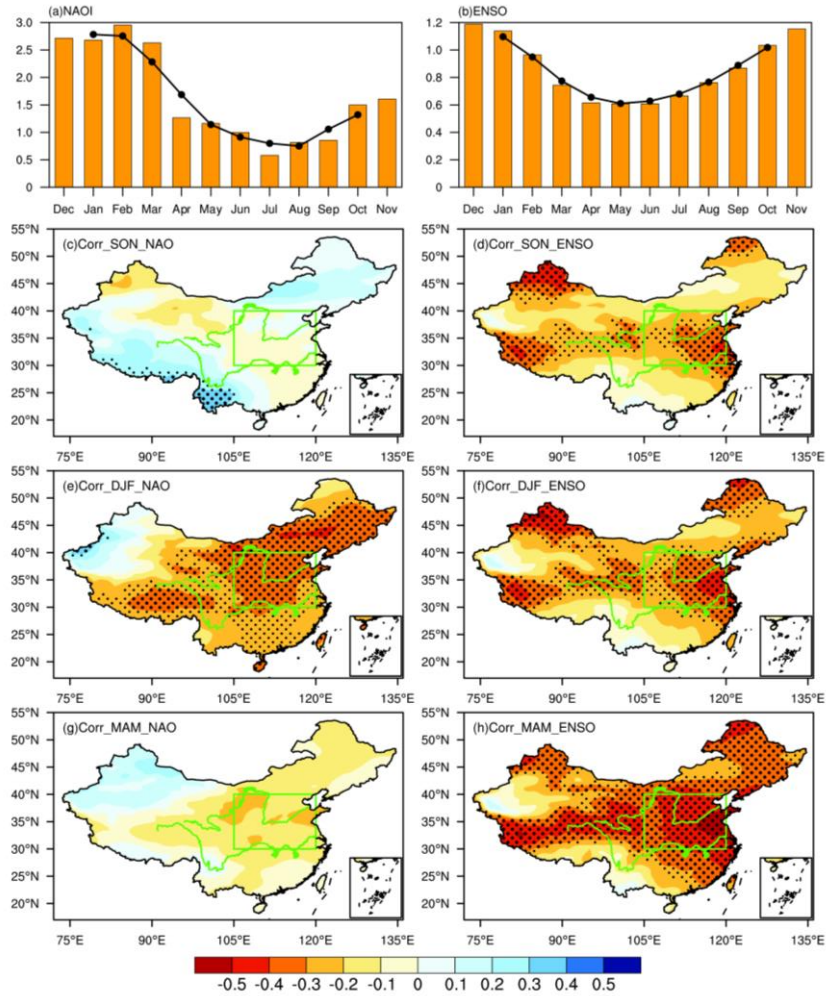
$$208 \quad W = \frac{pcos\varphi}{2|\mathbf{U}|} \cdot \left(\begin{aligned} & \frac{U}{a^2cos^2\varphi} \left[\left(\frac{\partial\psi'}{\partial\lambda} \right)^2 - \psi' \frac{\partial^2\psi'}{\partial\lambda^2} \right] + \frac{V}{a^2cos\varphi} \left[\frac{\partial\psi'}{\partial\lambda} \frac{\partial\psi'}{\partial\varphi} - \psi' \frac{\partial^2\psi'}{\partial\lambda\partial\varphi} \right] \\ & \frac{U}{a^2cos\varphi} \left[\frac{\partial\psi'}{\partial\lambda} \frac{\partial\psi'}{\partial\varphi} - \psi' \frac{\partial^2\psi'}{\partial\lambda\partial\varphi} \right] + \frac{V}{a^2} \left[\left(\frac{\partial\psi'}{\partial\varphi} \right)^2 - \psi' \frac{\partial^2\psi'}{\partial\varphi^2} \right] \\ & \frac{f_0^2}{N^2} \left\{ \frac{U}{acos\varphi} \left[\frac{\partial\psi'}{\partial\lambda} \frac{\partial\psi'}{\partial z} - \psi' \frac{\partial^2\psi'}{\partial\lambda\partial z} \right] + \frac{V}{a} \left[\frac{\partial\psi'}{\partial\varphi} \frac{\partial\psi'}{\partial z} - \psi' \frac{\partial^2\psi'}{\partial\varphi\partial z} \right] \right\} \end{aligned} \right) \quad (3)$$

209 In the expression, p , φ , λ , f_0 , and a represent the geopotential height, latitude, longitude,
 210 coriolis parameter, and Earth's radius, respectively. $\psi' = \Phi'/f$ (where Φ represents the
 211 geopotential) denotes the disturbance of the quasi-geostrophic stream function relative to the
 212 climatology. The basic flow field $\mathbf{U} = (U, V)$ denotes the climatic field, where U and V indicate
 213 the zonal and meridional velocities, respectively.

214 3. Results

215 3.1 Impacts of NAO and ENSO on the spring dust in North China

216 The standard deviation of the NAO peaks during December, January, and February. By
 217 analyzing the three-month running average standard deviation, it is seen the maximum occurs during
 218 winter. This indicates that winter NAO exhibits stronger variability compared to other seasons
 219 (Figure 2a). Similarly, ENSO shows larger variation during winter (Figure 2b). Previous studies
 220 have found that preceding NAO and ENSO play important roles in impacting the following climate
 221 over North China, particularly the cross-seasonal impacts (e.g., Zheng et al., 2016; Feng et al., 2019;
 222 Sun et al., 2021). We have examined the roles of previous autumn, winter and simultaneous spring
 223 NAO and ENSO on the spring dust aerosols over North China. It is found that the most significant
 224 influences of NAO and ENSO on the spring dust aerosols occurs when the NAO and ENSO leading
 225 one season (Figures 2c-h). Therefore, the roles of previous winter NAO and ENSO on the spring
 226 dust aerosols over North China are discussed.

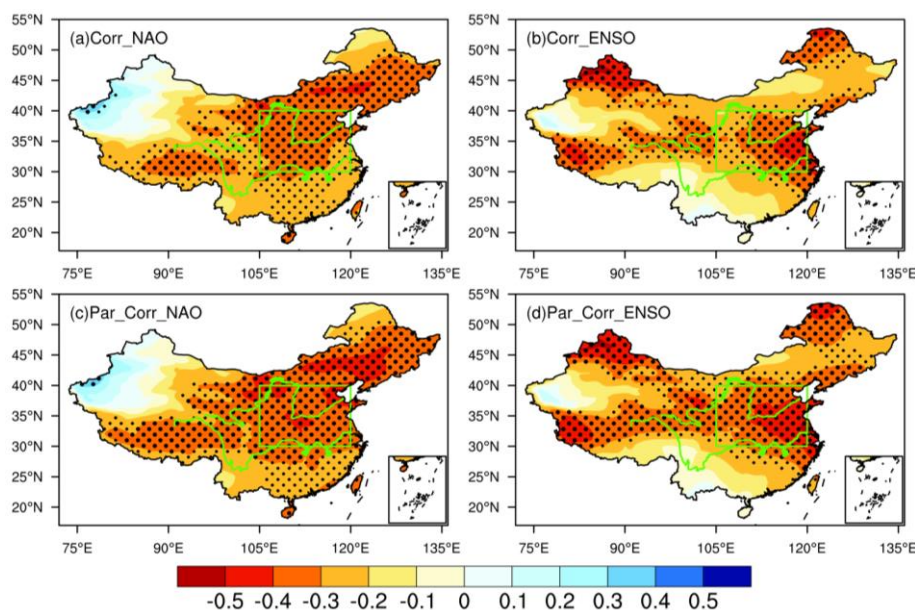


227

228 **Figure 2.** The monthly standard deviation of (a) NAOI and (b) Niño3.4 index, respectively. Black
 229 line represents three-month running average of standard deviation. (c) Spatial distribution of
 230 correlation coefficients between the previous autumn NAOI and spring dust content . (d) As in (c),
 231 but with Niño3.4 index. (e-f) and (g-h), as in (c-d), but for the correlations with previous winter and
 232 simultaneous spring NAOI and Niño3.4 index, respectively. The green box represents North China.
 233 Thick and fine stippled areas are statistically significant at the 0.05 and 0.1 level, respectively. The
 234 green lines in (c-h) represent the Yellow River (northern one) and the Yangtze River (southern one),
 235 respectively.

236 Previous studies have highlighted the significant impacts of NAO (e.g., Wu et al., 2009; Zheng
 237 et al., 2016a; Wang et al., 2018) and ENSO (e.g., Zhao et al., 2016; Zhang et al., 2016; Feng et al.,
 238 2020) on the climate anomalies over China. To investigate their effects on the spring dust, the
 239 correlations between the previous winter NAO/ENSO and following spring dust content are
 240 examined (Figure 3). Significant negative correlations are observed over North China between
 241 NAOI and dust content. Similar relationship is seen in the ENSO case. This result indicates that
 242 lower (higher) dust content is expected when the NAO and ENSO are in the positive (negative)
 243 phases (Figures 3a-b). Notably, Meanwhile, the NAOI/Niño3.4 index is significantly correlated with

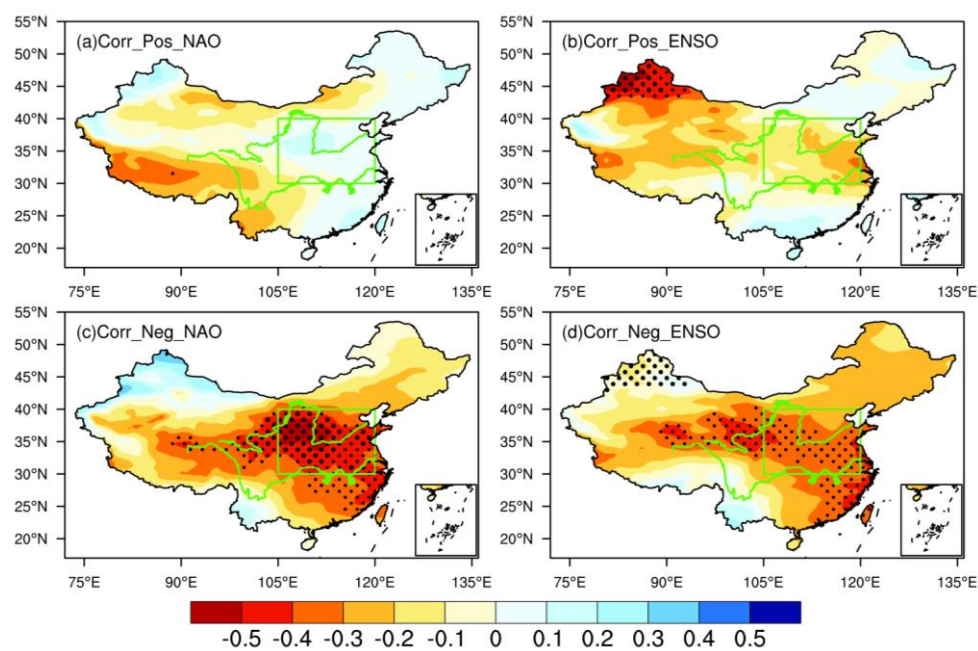
244 the areal averaged spring dust content over North China (SDI), with correlation coefficient of -0.36/-
 245 0.35. Considering the significant interaction between NAO and ENSO (López-Parages et al., 2015;
 246 Zhang et al., 2015), to detect their independent effects on the dust content, the partial correlation
 247 between NAO (ENSO) and dust content after removing the influence of the ENSO (NAO) are
 248 provided. The results indicate that the significant correlation regions between dust content and either
 249 the NAO or ENSO do not show little change significantly after removing the influence of the other.
 250 These findings suggest a stable and significant connection between the previous winter NAO and
 251 ENSO and the dust content in North China (Figures 3c-d).



252
 253 **Figure 3.** (a) Spatial distribution of correlation coefficients between the previous winter NAOI and
 254 spring dust content. (b) As in (a), but with Niño3.4 index. (c) As in (a), but for the partial correlation
 255 after removing the effect of ENSO. (d) As in (c), but after removing the effect of NAO. The green
 256 box represents North China. Thick and fine stippled areas are statistically significant at the 0.05 and
 257 0.1 level, respectively. The green lines represent the Yellow River (northern one) and the Yangtze
 258 River (southern one), respectively.

259 Previous studies have indicated that the development rate, intensity variations, and the spatial
 260 structure of NAO exhibit distinct asymmetric characteristics between different phases (Feldstein,
 261 2003; Jia et al., 2007). Furthermore, the influence of NAO on the EAWM is more pronounced during
 262 its negative phase (Sung et al., 2010). Similarly, both observational facts and model experiments
 263 suggest that El Niño and La Niña, as the positive and negative phases of ENSO, are not simply
 264 mirror images of each other. The SST anomalies in the tropical Pacific associated with ENSO exhibit
 265 significant asymmetry in terms of meridional range (Zhang et al., 2009), amplitude (Su et al., 2010),
 266 zonal propagation (McPhaden and Zhang, 2009), as well as climate impact (Feng and Li, 2011;
 267 Feng et al., 2020) under El Niño and La Niña conditions. Consequently, we further analyzed the

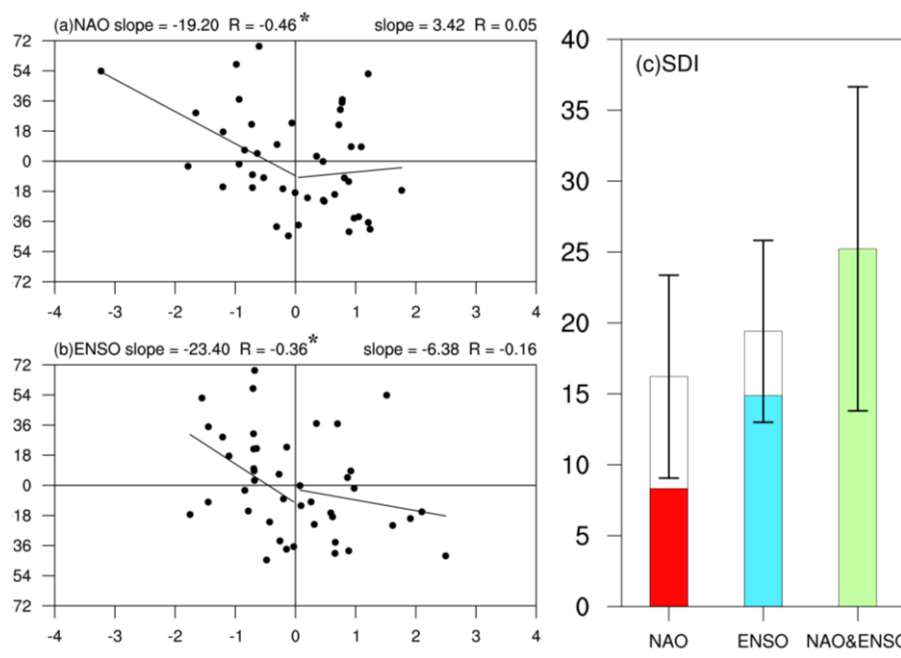
268 connection between NAO/ENSO and spring dust but in different phases. The results indicate that
 269 the relationship between NAO/ENSO and dust in North China also exhibits significant asymmetry,
 270 i.e., with weaker (stronger) correlations during positive (negative) phases of NAO and ENSO
 271 (Figure 4), where significant correlations only appear in the negative phases of NAO and ENSO.
 272 Based on the scatter distribution of SDI under different phases of NAO and ENSO, it is noted that
 273 the correlation coefficients between NAOI and SDI during the positive and negative phases of NAO
 274 are -0.46 and -0.05, respectively, indicating that the significant influence of NAO on the dust in
 275 North China mainly occurs during its negative phase (Figure 5a). Similarly, the correlation
 276 distribution between the ENSO and SDI also shows that the influence of ENSO is more pronounced
 277 during its negative phase (Figure 5b). These results indicate that the impacts of previous winter
 278 NAO and ENSO on the spring dust content in North China exhibit asymmetrical characteristics,
 279 significant effects mainly manifested during their negative phases.



280
 281 **Figure 4.** Spatial distribution of correlation coefficients between (a) positive and (c) negative NAOI
 282 values and dust content. (b) and (d) as in (a) and (b), respectively, but for the Niño3.4 index. The
 283 green box represents North China. Thick and fine stippled areas are statistically significant at the
 284 0.205 and 0.1 level, respectively. The green lines represent the Yellow River (northern one) and the
 285 Yangtze River (southern one), respectively.

286 The synergistic effects of climate variabilities from mid-high latitudes and tropics are pivotal
 287 mechanisms affecting the weather and climate in East Asia (Feng et al., 2019; Li et al., 2019).
 288 Correspondingly, we will examine whether the negative phases of previous winter NAO and ENSO
 289 exert synergistic effects on the following spring dust content in North China. As shown in Figure
 290 5c, when the NAO is in its negative phase (Table 1; white bar in Figure 5c labeled NAO), the value

291 of anomalous dust content over North China is $+16.21 \text{ mg}\cdot\text{m}^{-2}$, whereas it is $+8.32 \text{ mg}\cdot\text{m}^{-2}$ for the
 292 case that negative NAO occurred alone (red bar in Figure 5c). Similarly, the value of dust content
 293 anomalies over North China in the negative ENSO phase is greater than that when negative ENSO-
 294 occurred alone ($+19.40 \text{ mg}\cdot\text{m}^{-2}$ vs. $+14.88 \text{ mg}\cdot\text{m}^{-2}$). When the NAO and ENSO both are in negative
 295 phases (Table 1), the value of dust content anomalies ($+25.23 \text{ mg}\cdot\text{m}^{-2}$) is much greater than the
 296 situation when one of them is in the negative phase (green bar in Figure 5c). That is the negative
 297 phases of previous winter NAO and ENSO demonstrate synergistic effects on the spring dust
 298 activities in North China. Therefore, three categories, i.e., the NAO (ENSO) is in its negative phase,
 299 and both the NAO and ENSO are in the negative phases simultaneously (Table 1) are discussed in
 300 the context to elucidate the relevant processes of the synergistic effects of NAO and ENSO on the
 301 dust content over North China.



302
 303 **Figure 5.** Scatterplots of the spring dust content in North China against previous winter (a) NAOI
 304 and (b) Niño3.4 index. Also shown are lines of best fit for positive and negative NAO/Niño3.4 index
 305 values and correlation coefficients (R), slope (slope), * indicates significant at the 0.21 level. (c)
 306 Spring dust content over North China during the negative NAO, negative ENSO phases, and
 307 concurrent negative phases of NAO and ENSO (unit: $\text{mg}\cdot\text{m}^{-2}$). White bars represent negative phases
 308 of the NAO and ENSO, red and blue bars indicate solo negative NAO and ENSO years, and green
 309 bar is the negative NAO and ENSO co-occurring years.

310 **Table 1.** The events of NAO and ENSO classified by three categories

Scenarios	Years	Numbers
NAO	1980,1982,1985,1986,1987,1996,1998,2001, 2003,2004,2006,2010,2011,2013,2021	15
ENSO	1984,1985,1986,1989,1996,1999,2000,2001,	16

311 3.2 Impacts of NAO and ENSO on the environmental variables

312 To examine the anomalous characteristics associated with NAO and ENSO, the circulation
 313 anomalies in their negative phases, as well as in their co-~~occur~~occurring negative phases (Table 1)
 314 are analyzed. In the upper troposphere (200 hPa), the zonal wind is strengthened over the northwest
 315 of China and Mongolia during the negative NAO phase (Figure 6a), with evident positive anomalies
 316 centered on Mongolia, ~~reaching a maximum value of $+1.5 \text{ m}\cdot\text{s}^{-1}$~~ . In the case of negative ENSO
 317 phase, the upper-level zonal wind also shows an intensification over the northwest region of China
 318 and Mongolia, ~~with a maximum value of $+2 \text{ m}\cdot\text{s}^{-1}$~~ (Figure 6d). The intensification of upper-level
 319 zonal wind boosts the upper-level momentum, which is subsequently transferred downward to the
 320 mid-lower troposphere through vertical circulation (Wu et al., 2016; Li et al., 2023), causing windy
 321 weather in the surface dust source regions, facilitating dust lifting and transport activities, thereby
 322 promoting the occurrence of dust weatheractivities in the downstream North China. When both the
 323 NAO and ENSO are in their negative phases, the main positive anomaly center appears over North
 324 China, ~~reaching a maximum value of $+3 \text{ m}\cdot\text{s}^{-1}$~~ , which is stronger than the situation in either the
 325 NAO or ENSO. This result implies the synergistic effects of NAO and ENSO on the upper-level
 326 zonal wind, facilitating an enhanced transport of dust from its source regions to North China,
 327 consequently triggering the onset of dust weatheractivities conditions in North China (Figure 6g).

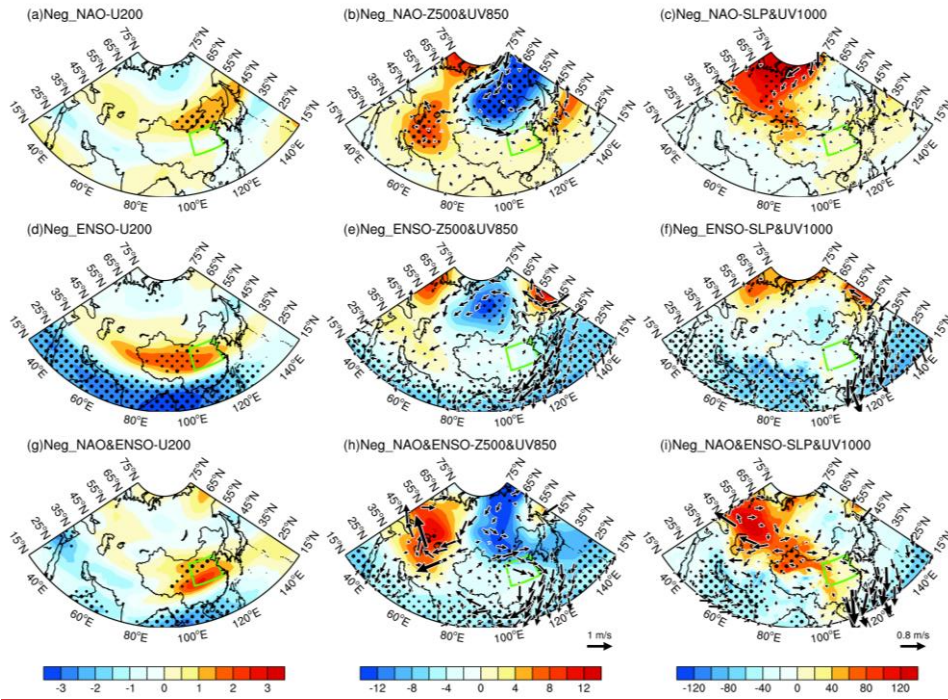
328 Subsequent analysis delved into the anomalous distribution of the circulation field in the mid
 329 and lower troposphere. In the negative NAO phasesituation, a pronounced “trough-ridge” anomaly
 330 pattern emerges in the mid-latitude region, characterized by a trough in Siberia and a ridge in the
 331 Middle East, ~~with their anomalous intensities reaching -12 gpm and $+10 \text{ gpm}$, respectively~~ (Figure
 332 6b). This atmospheric configuration fosters a dominant meridional circulation in the mid-high
 333 latitude region, thereby facilitating the enhanced transport of cold air from the north. Such a
 334 southward incursion of cold air serves to strengthen the surface wind speeds, and to promote the
 335 uplift and transport of dust from the source regions. In the negative ENSO phasesituation, although
 336 the mid-latitude region exhibits a similar trough-ridge pattern, more pronounced circulation
 337 anomalies are observed over the WNP. At this time, the region is predominantly under the influence
 338 of northeasterly winds on its western flank, manifesting cyclonic circulation anomalies (Figure 6e),
 339 consistent with previous research results (Ke et al., 2023). This abnormal circulation will hinder the
 340 northward transport of warm and moist air from the South China Sea and the Bay of Bengal,

341 diminishing the likelihood of interactions with cold air from the north, thus reducing the possibility
342 ~~for the formation of forming~~ of stationary fronts and precipitation. The decrease in precipitation
343 weakens the wet deposition effect (Zheng et al., 2016b; Huang et al., 2021), favoring the occurrence
344 of dust ~~weather activities~~ in the region. When both the NAO and ENSO are simultaneously ~~in their~~
345 ~~negative phases occurred~~, the meridional circulation in the mid-latitude region is enhanced ~~with the~~
346 ~~maximum anomalies of the trough and ridge reaching -12 gpm and +12 gpm, respectively~~ (Figure
347 4h6h). Furthermore, the southward shift of the trough-ridge pattern leads to a more significant
348 increase in wind speed in the upstream dust source regions of North China, providing a more
349 substantial source of dust for North China. Meanwhile, the presence of a cyclonic circulation
350 anomalies over the WNP reduces the transport of warm and moist air from the south, which is
351 unfavorable for precipitation, thereby lowering the wet deposition effect on dust and further favoring
352 the onset and intensification of dust activities in North China.

353 As for the SLP, significant positive SLP anomalies appear in Eastern Europe and Russia during
354 negative NAO ~~phases situation~~, indicative of an intensified Siberian High (SH), which extends
355 southward to the dust source regions upstream of North China (Figure 6c). The intensification of
356 the SH ~~is~~ typically accompanied ~~with by~~ strong northerlies and dry conditions, favoring ~~for~~ the
357 transport of dust, thereby supplying abundant material sources for dust activities in North China. In
358 the negative ENSO ~~phase case~~, although the high-latitude region exhibits a weaker SH signal, similar
359 to the ENSO influence on the circulation pattern in the middle and lower troposphere, more
360 significant circulation anomalies occur over the WNP. This cyclonic circulation ~~anomalies~~ inhibit
361 the northward transport of warm and moist air from the south, leading to ~~poorer~~ ~~unfavorable~~
362 precipitation conditions in North China (Figure 6f). When both the NAO and ENSO are in their
363 negative phases, the intensify and extent of the SH are more pronounced compared to that when the
364 NAO sole is in negative phase. ~~Additionally~~, cyclonic circulation ~~anomalies persist~~ over the WNP,
365 which ~~is are~~ conducive to the occurrence of dust events in North China (Figure 6i).

366 The results suggest that when both the NAO and ENSO are in their negative phases, synergistic
367 effects ~~emerges emerge~~, rendering the atmospheric circulation in the troposphere more conducive to
368 the occurrence of dust events in North China. The synergistic effects may be due to the superposition
369 and interaction of various atmospheric levels and regional characteristics modulated by the NAO
370 and ENSO, thereby forming more favorable circulation conditions for dust activities in North China.

371



372

373 **Figure 6.** Upper, the composite anomalies of (a) 200 hPa zonal wind (shading, unit: $\text{m}\cdot\text{s}^{-1}$), (b) 500
 374 hPa geopotential height (shading, unit: gpm) and 850 hPa wind field (arrows, unit: $\text{m}\cdot\text{s}^{-1}$), (c) sea-
 375 level pressure (shading, unit: Pa) and 1000 hPa wind field (arrows, unit: $\text{m}\cdot\text{s}^{-1}$) during the negative
 376 NAO phases. Middle-Lower, as in the upper, but during the negative ENSO phases and co-occurred
 377 negative phases of NAO and ENSO, respectively. The green arrows are box represents North China.
 378 Only wind anomalies statistically significant at the 0.1 level are shown. Thick and fine stippled areas
 379 are statistically significant at the 0.05 and 0.1 level, respectively.

380

381

382

383

384

385

386

387

388

389

390

391

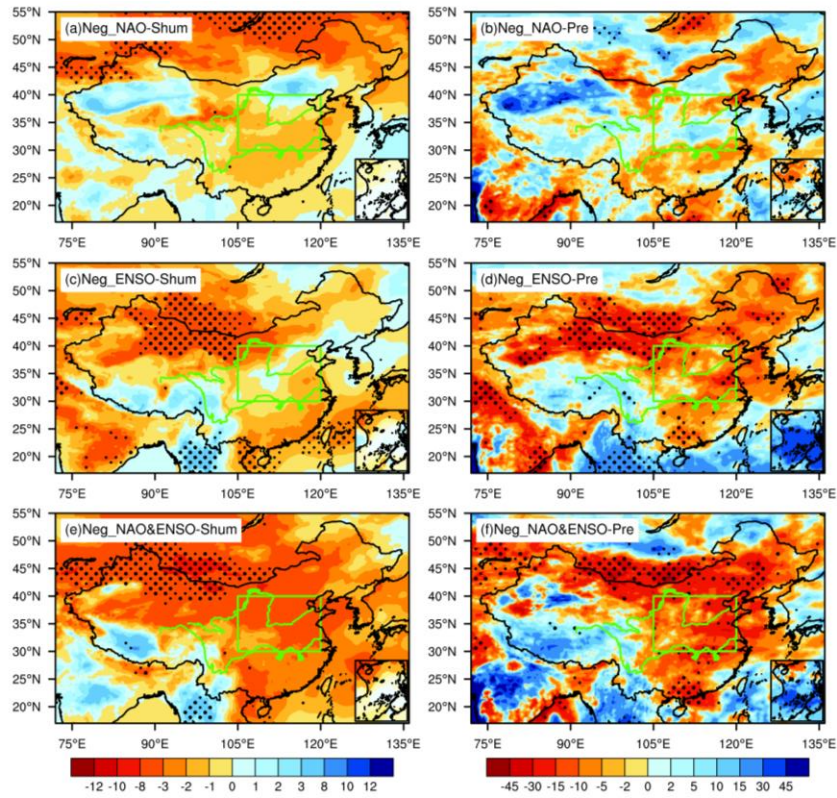
392

393

Dust activities are multifaceted ~~phenomenon~~phenomena related to large-scale circulation patterns, and significantly influenced by local surface conditions and meteorological processes. Surface properties and local meteorological factors play a role in the initiation, development, and dissipation of dust activities (e.g., Liu et al., 2004; Yao et al., 2021; Huang et al., 2021). In particular, humidity and precipitation play decisive roles in determining the frequency and intensity of dust activities (Prospero et al., 1987; Kim and Choi, 2015). Low humidity leads to drier soil conditions in the dust source regions, reducing the cohesion between soil particles and facilitating ~~–~~dust lifting and transport activities (Csavina et al., 2014), and vice versa. Similarly, the amount of precipitation directly affects the wet deposition process of dust. ~~Low~~Less precipitation weakens the wet deposition, ~~resulting in~~associated with relatively ~~stronger~~higher dust content (Zheng et al., 2016b). Therefore, we further analyzed their potential impacts on the humidity and precipitation. When the NAO is in its negative phase, humidity in the spring dust source regions and North China is generally reduced, particularly in areas near the dust source regions, indicating that these areas are conducive to dust transport and prone to causing dust ~~weather~~activities in North China (Figure 7a). As for the

394 precipitation, there is more spring precipitation in the northwest region of China, while precipitation
395 in the Mongolia and the North China is relatively less (Figure 7b). In the negative ENSO phase, the
396 variation in humidity is similar to that during the negative NAO phase, but with a greater amplitude
397 (Figure 7c), indicating that ENSO has a stronger impact on the humidity conditions in North China.
398 Moreover, the precipitation shows a significant ~~abnormal~~ decrease over Mongolia and North China,
399 which is highly conducive to dust activities ~~and the generation of dust weather~~ (Figure 7d). When
400 both the NAO and ENSO are in the negative phases, the humidity anomalies in the dust source
401 regions and North China are more intense than the individual factor (Figure 7e). The variation in
402 precipitation is similar to those in humidity, the reduction in precipitation in the dust source regions
403 and North China exceeds the sole role (Figure 7f). The aforementioned analysis indicates that the
404 NAO and ENSO can modulate humidity and precipitation, ultimately affecting dust
405 ~~weather activities~~. During the negative NAO case, the diminished atmospheric pressure gradient in
406 the mid-high latitude regions of North Atlantic leads to the intensification and southward shift of
407 the SH (Zhou et al., 2023), accompanied with strong wind, making the environment drier and
408 conducive to dust lifting and transport in the dust source regions. In the negative ENSO case, the
409 upper atmosphere over the WNP is dominated by significant negative anomalies in geopotential
410 height and northeasterly winds (Zhang et al., 2015), reducing moist transport. When the NAO and
411 ENSO both are in negative phases, their regulation of atmospheric circulation produces synergistic
412 effects, further influencing the variations of humidity and precipitation, thereby promoting the
413 occurrence and development of dust activities in North China.

414



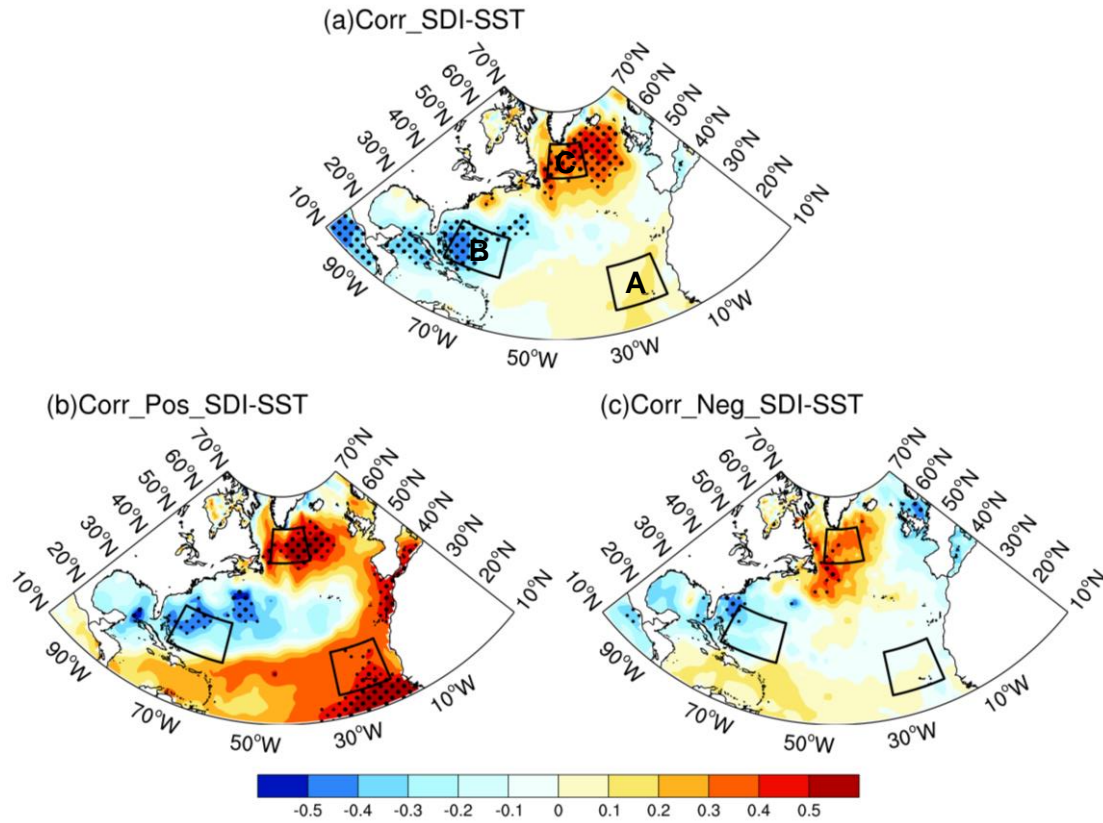
415

416 **Figure 7.** As in Figure 6, but for the composite percentage anomalies of (Left) special humidity and
 417 (Right) precipitation.

418 **3.3 Physical Mechanisms of the NAO and ENSO on the dust** 419 **weather activities**

420 The above results demonstrate that the previous winter NAO and ENSO exert significant
 421 impacts on the spring dust activities in North China. Consequently, an examination of the underlying
 422 physical mechanisms is warranted. Given the relatively short memory of NAO as an atmospheric
 423 phenomenon, we will employ the concept of ocean-atmosphere coupling bridge to elucidate the
 424 involved processes. The previous ENSO signal can alter the atmospheric circulation over the WNP
 425 through the persistent impact of SST, thereby significantly affecting subsequent weather and climate
 426 in China (e.g., Wu et al., 2017; Kim and Kug, 2018; Jiang et al., 2019). The tripole configuration of
 427 SST is the leading mode of SST variation in the North Atlantic, and its variabilities are closely
 428 associated with the NAO (Wu et al., 2009), allowing the previous NAO signal to exert a long-term
 429 influence on the subsequent weather and climate in China (e.g., [Chen et al., 2020](#); [Wu and Chen,](#)
 430 [2020](#); [Song et al., 2022](#)). The variation of SDI is linked with an anomalous tripole SST in the North
 431 Atlantic (Figure 8a), paralleling with the SST anomalies accompanied with the negative phase of
 432 NAO. Therefore, the North Atlantic tripole index (NATI) is defined to depict the characteristics of

433 SST anomalies (Equations 4-7), as well as the relationships among the NAOI, NATI, and SDI are
 434 explored. The correlation analysis between the high and low years of SDI and NATI reveals a
 435 pronounced difference, indicating an asymmetric correlation (Figures 8b-c). Specifically, the
 436 significant relationship between SDI and NATI only existed in the positive SDI years, implying that
 437 the occurrence of NATI would ~~connected~~connect with more dust ~~weather~~activities over North China.



438
 439 **Figure 8.** (a) Spatial distribution of the correlation coefficients between the spring SDI and
 440 simultaneous SST. (b)-(c) As in (a), but for the positive and negative phase of SDI. Thick and fine
 441 stippled areas are statistically significant at the 0.05 and 0.1 level, respectively. The black box
 442 represents NATI.

443
$$SST_A = [15-25^{\circ}N, 32-20^{\circ}W] \quad (4)$$

444
$$SST_B = [22-32^{\circ}N, 75-60^{\circ}W] \quad (5)$$

445
$$SST_C = [50-60^{\circ}N, 50-32^{\circ}W] \quad (6)$$

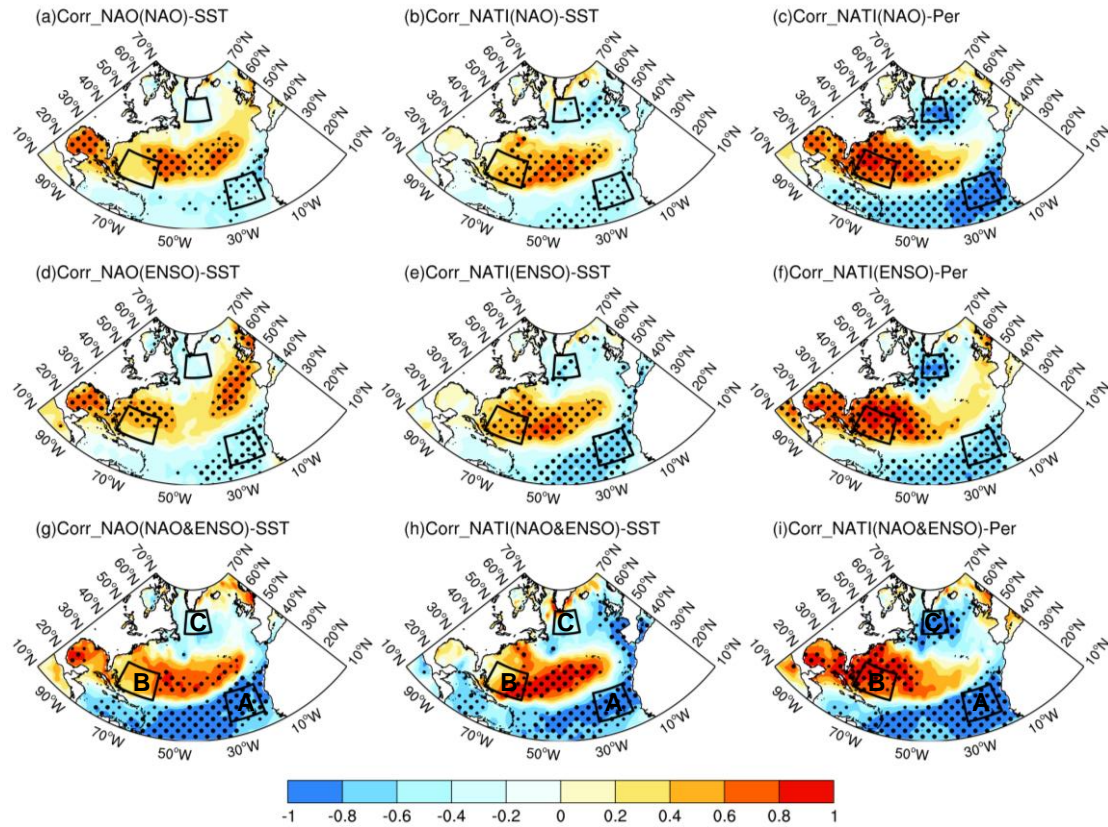
446
$$NATI = SST_B - \frac{1}{2}(SST_A + SST_C) \quad (7)$$

447 Subsequent analyses delved into the association between the previous winter NAO and the
 448 North Atlantic SST. It is seen that the correlation coefficients between the negative (positive) NAOI
 449 and NATI are 0.41(-0.09) (figures not shown), indicating that the influence of previous winter NAO
 450 on the following spring NATI only manifest during its negative phase. This elucidates the reason
 451 why the significant impact of NAO on the dust activities in North China only existed during its

452 negative phase. In the negative NAO phase, there is a notable correlation between the previous
453 winter NATI and the spring SST and SST_p (Figures 9b-c), indicating that the previous winter NATI
454 can persist into spring, in which the self-persistence of SST playing a crucial role. Similar findings
455 are observed during the negative phase of ENSO (Figures 9e-f) and when both the NAO and ENSO
456 occur simultaneously (Figures 9h-i).

457 The correlation between the previous winter NAO and North Atlantic SST reveals that in the
458 NAO negative situation (Figure 9a), the variation of NAO is linked with an anomalous tripole SST
459 pattern in the North Atlantic. Meanwhile, similar findings are observed during negative ENSO
460 situation (Figure 9d). This suggests that there may be positive feedback occurred between NAO and
461 North Atlantic SST during negative ENSO phase. When both the NAO and ENSO are in the
462 negative phases, the anomalous tripole SST pattern is more pronounced (Figure 9g). This further
463 elucidates that ENSO exerts a promoting effect on strengthening the connection between the
464 negative NAO and NATI, providing an explanation for the synergistic effects of the NAO and ENSO
465 on the dust ~~weather~~activities in North China. Additionally, the correlation coefficients between the
466 NAOI and NATI under different scenarios can illustrate the synergistic influence of the NAO and
467 ENSO on the persistence of SST anomalies (Table 2). Specifically, when the negative phase of NAO
468 and ENSO occur together, the correlation coefficients between the NAOI and NATI are greater than
469 those influenced by a single factor alone (Table 2). The impacts of previous winter NAO on the
470 spring dust activities over North China are mainly include. 1) The previous winter NAO would
471 stimulate the anomalous NAT SST pattern; 2) The NAT can last from previous winter to the
472 following spring due to the thermal persistence of the SST; 3) The spring NAT plays significant
473 modulation on the circulation pattern over North China through teleconnection wave trains, which
474 ultimately affects the spring dust activities over North China. It is seen from Table 2 that although
475 in the case of ENSO- phase and NAO- & ENSO- phase, the correlation coefficients of previous
476 winter NATI and spring NATI are same. However, the correlations between the NAOI and NATI is
477 higher during NAO- & ENSO- phase (0.66) than ENSO- phase (0.52), highlighting the significant
478 role of NAO on the NAT in the case of NAO- & ENSO- phase. The above discussion illustrates the
479 synergistic effect of NAO and ENSO on the dust activities over North China.

480



481

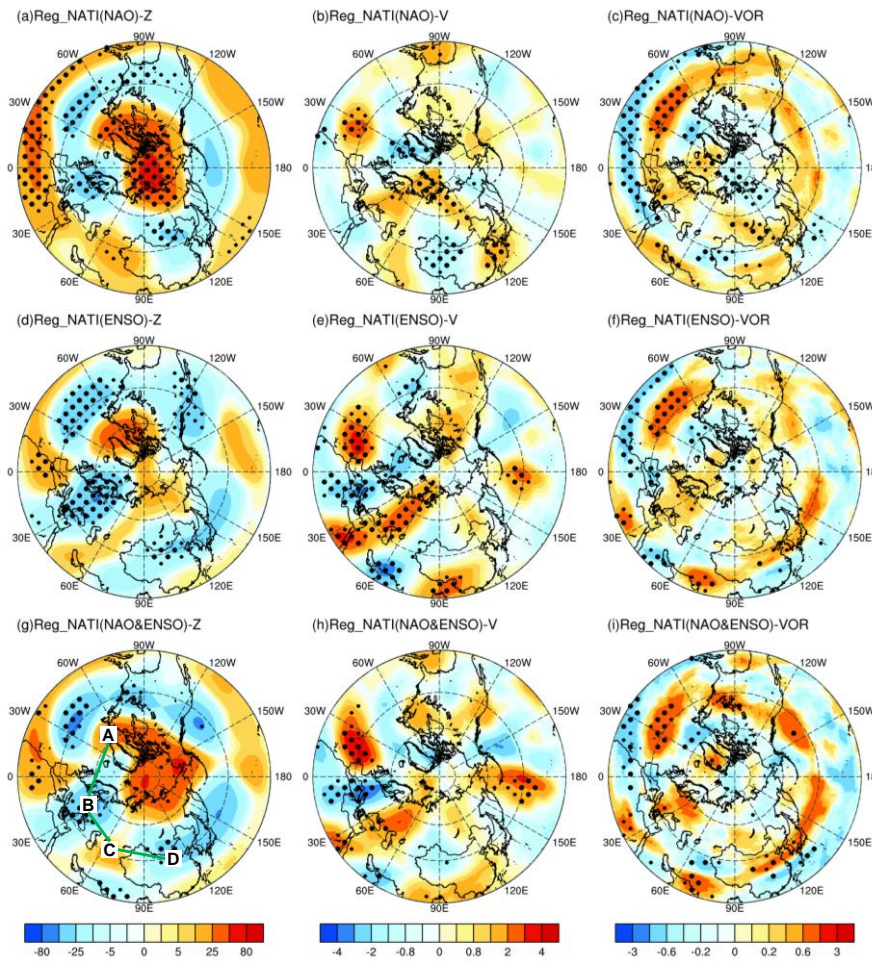
482 **Figure 9.** Upper, correlation distributions of the (a) winter NAOI with winter SST, (b) winter NATI
 483 with spring SST, and (c) winter NATI with SST_p during negative NAO phases. Middle-Lower, as
 484 in the upper, but during the negative ENSO phases and concurrent negative phases of NAO and
 485 ENSO, respectively. Thick and fine stippled areas are statistically significant at the 0.205 and 0.1
 486 level, respectively. The black box represents NATI.

487 **Table 2.** Correlation coefficients between the NAOI and NATI in three different categories. *
 488 indicates significant at the 0.1 level.

Scenarios	DJF_NAO & DJF_NATI	DJF_NATI & MAM_NATI
NAO ⁻ phase	0.41*	0.51*
ENSO ⁻ phase	0.52*	0.69*
NAO ⁻ & ENSO ⁻ phase	0.66*	0.69*

489 The NAO preserves its anomalous signal within the tripole SST during the previous winter,
 490 and releases the anomalous signal in the following spring. Given the distance across the entire
 491 Eurasian continent between the North Atlantic and North China, the role of teleconnection wave
 492 trains is particularly important in influencing dust activities over North China. Figure 10a illustrates
 493 the geopotential height field at 200 hPa regressed onto the spring NATI during negative NAO case.
 494 This reveals a pronounced north-south reversed dipole pattern in the North Atlantic, i.e., negative
 495 over Azores and positive over Iceland, representing a typical negative NAO structure (e.g., Wallace
 496 and Gutzler, 1981; Hurrell, 1995; Li and Wang, 2003). Meanwhile, a positive-negative-positive

497 teleconnection wave train structure centered around eastern Europe, Middle East, and North China
 498 is observed, suggesting that the disturbance energy propagates downstream from the North Atlantic
 499 through waveguide effects, leading to anticyclonic circulation anomalies in North China. Similar
 500 teleconnection wave-train propagation characteristics are also observed in the 200 hPa meridional
 501 wind and vorticity fields (Figures 10b-c). During the negative ENSO case, modulated by the NATI,
 502 analogous teleconnection structures are also seen in the circulation field (Figures 10d-f). Notably,
 503 when the NAO and ENSO are both in their negative phases, the teleconnection structure reflected
 504 in the circulation field is more pronounced than when only one factor is dominated (Figures 10g-i),
 505 confirming the synergistic effects of both factors on the circulation processes affecting dust activities
 506 in North China.



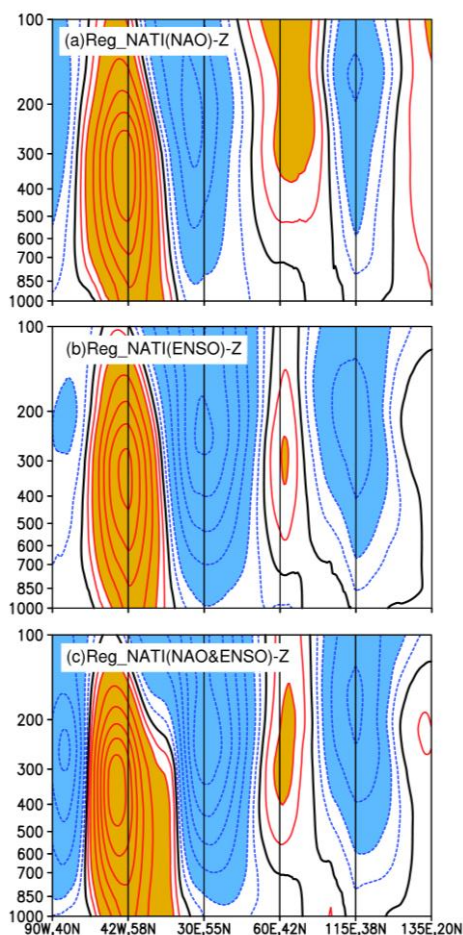
507

508 **Figure 10.** Upper, regression distribution of spring NATI against the spring (a) geopotential height
 509 (unit: gpm), (b) meridional wind (unit: $\text{m}\cdot\text{s}^{-1}$), and (c) vorticity (unit: $10^{-5}\cdot\text{m}\cdot\text{s}^{-1}$) at 200 hPa during
 510 the negative NAO phase. Middle-lower, as in the upper, but during the negative ENSO phases and
 511 concurrent negative phases of NAO and ENSO, respectively. Regression fields multiplied by -1.
 512 Thick and fine stippled areas are statistically significant at the 0.05 and 0.1 level, respectively.

513

To further examine the impact mechanisms of NAO and ENSO on the spring dust activities in

514 North China, based on the propagation characteristics of the teleconnection wave train shown in
 515 Figure 10, the distribution of cross-section of the geopotential height field is presented (Figure 11).
 516 When both the NAO and ENSO are in their negative phases, the NATI anomalies correspond to the
 517 teleconnection wave train extending from the upper to lower troposphere, which is specifically
 518 characterized by a positive-negative-positive tripole pattern. This wave train propagates from the
 519 North Atlantic, traversing eastern Europe and Middle East, and ultimately influencing circulation
 520 processes associated with the dust weatheractivities over North China. Furthermore, the analysis of
 521 cross-section at different levels of the troposphere reveals that under the negative NAO and ENSO
 522 situations, the teleconnection wave train excited by the NATI exhibits quasi-barotropic features,
 523 with this anomalous structure being primarily concentrated in the middle-upper troposphere. When
 524 the NAO and ENSO are simultaneously in their negative phases, the intensity and scope of the
 525 teleconnection wave train are significantly enhanced and expanded compared to the influence of a
 526 single factor (Figure 9c), demonstrating synergistic effects.

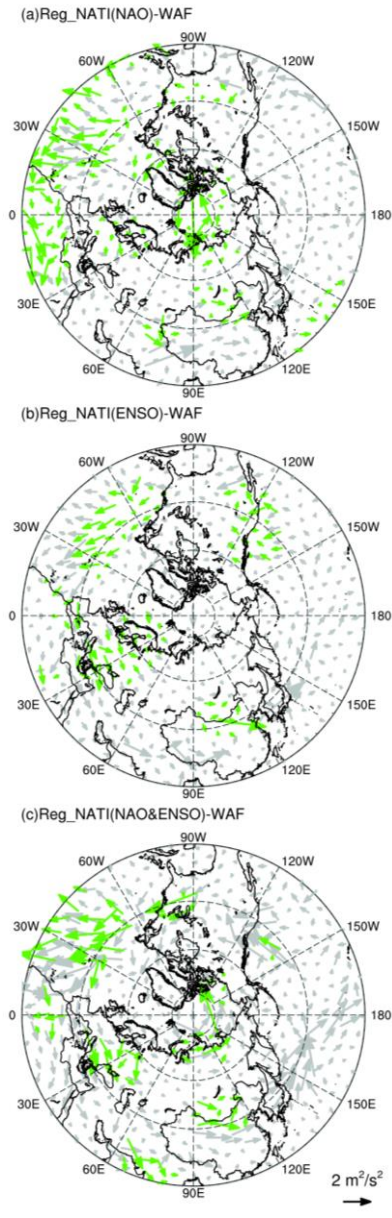


527
 528 **Figure 11.** Vertical section of regression of spring NATI against the geopotential height along the
 529 solid line labeled A (42°W, 58°N), B (30°E, 55°N), C (60°E, 42°N), and D (115°E, 38°N) in Figure
 530 10g for (a) negative NAO case in the previous winter. (b)-(c) as in (a), but during the negative ENSO

531 case and co-occurring negative phases of NAO and ENSO, respectively (unit: gpm). Regression
532 fields have multiplied by -1. Shading indicates the absolute value is greater than 10 gpm.

533 To provide a more comprehensive analysis of the transport process of disturbance energy in
534 the atmosphere, the horizontal distribution of the WAF associated with spring NATI variations is
535 further examined. Under the scenario that either the NAO or ENSO is in their negative phases, WAF
536 can be clearly observed to originate from the North Atlantic, traverse the Eurasian continent, and
537 extend to the North China (Figures 12a-b). When both factors occur simultaneously, not only is the
538 transport intensity of WAF enhanced, but its impact range on the dust weatheractivities in North
539 China is also broadened (Figure 12c). Through the analysis of teleconnection wave trains and WAF,
540 it is determined that the synergistic effects not only enhance the disturbance intensity in the
541 atmosphere but also expand impact rangeimpacted extent, thereby promoting the occurrence and
542 development of spring dust weatheractivities in North China. The enhancement and expansion of
543 atmospheric disturbances may be related to large-scale circulation anomalies and local climate
544 condition changes induced by the synergistic effects of the NAO and ENSO, which in turn affect
545 the transport and deposition processes of dust.

546



547

548 **Figure 12.** As in Figure 10, but for the regression distribution of spring NATI against the T-N wave
 549 activity flux (units: $\text{m}^2 \cdot \text{s}^{-2}$). Regression fields have multiplied by -1. Green arrows are statistically
 550 significant at the 0.1 level.

551 **4. Conclusions and discussions**

552 The NAO and ENSO exert significant impacts on climate variability in China (e.g., Zhang et
 553 al., 2016; Wang et al., 2018; Feng et al., 2020). Although North China is not the primary dust source,
 554 ~~dusty disasters~~ dust activities are notably active during spring in this region. This study highlights
 555 that the previous winter NAO and ENSO exert essential influences on the following spring dust
 556 activities in North China. Their impacts are asymmetric, manifesting only when both are in their
 557 negative phases. Furthermore, the results indicate that NAO and ENSO in the negative phase have

558 synergistic effects on the spring dust activities in North China, promoting dust activities and with
559 greater impacts than their sole effect.

560 Under the regulatory influence of the negative phases of NAO and ENSO, the atmospheric
561 circulation in the troposphere from the lower to upper layers, exhibits anomalies. These include
562 variations in the upper-level zonal winds, mid-latitude trough-ridge systems, circulation over the
563 WNP, and the SH at the SLP. These variations promote the occurrence and development of dust
564 weather activities in North China. Simultaneously, accompanying anomalies in the atmospheric
565 circulation pattern also affect local meteorological factors, including humidity and precipitation,
566 which in turn impact the dust activities in North China. Notably, when both the NAO and ENSO
567 are in their negative phases, synergistic effects occur, making the anomalies in atmospheric
568 circulation from the lower to upper layers, as well as variations in humidity and precipitation, more
569 conducive to the occurrence of dust events in North China. The impact of NAO on the underlying
570 SST pattern is predominantly observed during its negative phase, elucidating why the NAO
571 significantly influences dust activities in North China only during its negative phase. Furthermore,
572 when both the NAO and ENSO simultaneously manifest in their negative phases, the teleconnection
573 wave trains and WAF stimulated from the North Atlantic are more intense, thereby more effectively
574 influencing dust activities in North China. This indicates the synergistic effects of the two
575 variabilities on dust activities over North China.

576 In the process where the previous winter NAO and ENSO affect the following spring dust
577 activities in North China, the persistence of anomalous NAT over North Atlantic plays an important
578 role. The previous winter NAO stores its signal in the NAT (Wu et al., 2009). Due to the persistence
579 of SST, the anomalous NAT can last from winter to spring (e.g., Wu et al., 2012; Zhang et al., 2021a;
580 Li et al., 2023). In spring, NAT regulates the circulation pattern in North China through
581 teleconnection wave trains, ultimately affecting the dust activities over North China. The signal of
582 previous winter ENSO can persist into spring, due to the persistence of SST, and it affects the dust
583 activities in North China through two pathways: i.e., directly influencing the dust activities in North
584 China by affecting the circulation anomalies over the WNP, and playing a facilitating role in the
585 process where the NAO excites NAT, thereby affecting the dust activities in North China. This
586 provides a plausible explanation for why the previous winter NAO and ENSO exert synergistic
587 effects on the following spring dust activities in North China.

588 This study investigated the impacts of NAO and ENSO on the dust activities in North China
589 and the involved physical processes, indicating that one season ahead signals provide as the useful

590 predictors for spring dust activities in North China. Future work will focus on developing a
591 prediction model using the NAO and ENSO as predictors and validating its prediction effectiveness.
592 Additionally, as previous studies have highlighted strong interdecadal variations in both the NAO
593 and ENSO (e.g., Woollings et al., 2015; Wang et al., 2023; Feng et al., 2024), it is of interest to
594 further detect whether the synergistic effects of NAO and ENSO on the dust activity over North
595 China experience interdecadal variations. However, due to the availability of dataset, the potential
596 impacts of the interdecadal variability of the NAO and ENSO on dust activities have not been
597 discussed in this study. Simultaneously, as reported that the state-of-art models can reproduce the
598 individual impact of NAO and ENSO on the dust activities in North China (Yang et al., 2022),
599 whether their synergistic effects on the dust ~~weather~~activities could be well simulated, requiring
600 further researches. Additionally, previous studies have indicated that the uncertainty in ENSO
601 ~~variability of ENSO~~ is likely to intensify/increase under the background of global warming (Cai et
602 al., 2021; Chen et al., 2024). Therefore, it is crucial to investigate the future changes in the NAO,
603 as well as future change of its synergistic effects with the ENSO on the dust activities, to better
604 understand the plausible trends of future dust activities in North China. The present study is focused
605 to period 1979-2022, due to the longevity of the MERRA-2 dust aerosol. There are only 7 co-
606 occurrence years of negative NAO and ENSO. The co-occurrence of negative NAO and ENSO
607 takes up to 17% of the whole study period. To be noted is that the sample are not long enough, it is
608 worthy to examine their joint impacts by employing longer datasets or models outputs, to further
609 detect their synergistic effects as well as any possible variations in their modulations. This study did
610 not discuss the potential impacts of interdecadal signals, such as the AMO, on dust activities in
611 China. The interdecadal variations of dust activities over China as well as its connection to the
612 interdecadal climatic variabilities will be discussed in future work.

613

614 **Code and data availability.** The MERRA-2 dust aerosol content dataset can be downloaded from
615 <https://disc.gsfc.nasa.gov/datasets?project=MERRA-2> (last access: 7 July 2024). The atmospheric
616 reanalysis datasets, including wind, geopotential height, and sea-level pressure, specific humidity,
617 precipitation, and vorticity field can be downloaded from
618 <https://cds.climate.copernicus.eu/#!/search?text=ERA5&type=dataset> (last access: 7 July 2024).
619 The oceanic reanalysis data can be downloaded from <https://www.metoffice.gov.uk/hadobs/hadisst>
620 (last access: 7 July 2024). The NAO indices defined by Li and Wang can be downloaded from
621 <http://lijianping.cn/dct/page/65610> (last access: 7 July 2024). The NAO indices produce by Hurrell

622 [and Jones can be downloaded from https://climatedataguide.ucar.edu/climate-data/hurrell-north-](https://climatedataguide.ucar.edu/climate-data/hurrell-north-atlantic-oscillation-nao-index-pc-based)
623 [atlantic-oscillation-nao-index-pc-based](https://climatedataguide.ucar.edu/climate-data/hurrell-north-atlantic-oscillation-nao-index-pc-based) (last access: 7 July 2024) and
624 <https://crudata.uea.ac.uk/cru/data/nao> (last access: 7 July 2024), respectively. The ENSO indices
625 [can be downloaded from https://psl.noaa.gov/data/timeseries/monthly/NINO34](https://psl.noaa.gov/data/timeseries/monthly/NINO34) (last access: 7 July
626 [2024](https://psl.noaa.gov/data/timeseries/monthly/NINO34)). Our results can be made available upon request.

627

628 **Author contributions.** JF and FLX conceptualized and designed the research. FLX and JF
629 synthesized and analyzed the data. FLX, SW, YL, and JF produced the figures. FLX and SW
630 contributed to the dataset's retrieval. All the authors discussed the results and wrote the paper.

631

632 **Competing interests.** The authors declare that they have no conflict of interest.

633

634 **Disclaimer.** Publisher's note: Copernicus Publications remains neutral with regard to jurisdictional
635 claims in published maps and institutional affiliations.

636

637 **Acknowledgements.** The authors would like to thank two anonymous reviewers and editor Marco
638 Gaetani for their useful comments and suggestions that contributed to improving the manuscript.
639 This work was jointly supported by the National Natural Science Foundation of China (42222501)
640 and the BNU-FGS Global Environmental Change Program (No. 2023-GC-ZYTS-03).

641

642 **References**

- 643 Abid, M. A., Kucharski, F., Molteni, F., Kang, I.-S., Tompkins, A. M., and Almazroui, M.: Separating the Indian and
644 Pacific Ocean Impacts on the Euro-Atlantic Response to ENSO and Its Transition from Early to Late Winter, *J.*
645 *Climate*, 34, 1531–1548, <https://doi.org/10.1175/JCLI-D-20-0075.1>, 2021.
- 646 Achakulwisut, P., Shen, L., and Mickley, L. J.: What Controls Springtime Fine Dust Variability in the Western United
647 States? Investigating the 2002–2015 Increase in Fine Dust in the U.S. Southwest, *J. Geophys. Res.-Atmos.*, 122,
648 <https://doi.org/10.1002/2017JD027208>, 2017.
- 649 Ayarzagüena, B., Ineson, S., Dunstone, N. J., Baldwin, M. P., and Scaife, A. A.: Intraseasonal Effects of El Niño–
650 Southern Oscillation on North Atlantic Climate, *J. Climate*, 31, 8861–8873, [https://doi.org/10.1175/JCLI-D-18-](https://doi.org/10.1175/JCLI-D-18-0097.1)
651 0097.1, 2018.
- 652 Cai, W. J., Santoso, A., Collins, M., Dewitte, B., Karamperidou, C., Kug, J.-S., Lengaigne, M., McPhaden, M. J.,
653 Stuecker, M. F., Taschetto, A. S., Timmermann, A., Wu, L. X., Yeh, S.-W., Wang, G. J., Ng, B., Jia, F., Yang, Y.,
654 Ying, J., Zheng, X. T., Bayr, T., Brown, J. R., Capotondi, A., Cobb, K. M., Gan, B. L., Geng, T., Ham, Y.-G.,
655 Jin, F. F., Jo, H.-S., Li, X. C., Lin, X. P., McGregor, S., Park, J.-H., Stein, K., Yang, K., Zhang, L., and Zhong,
656 W. X.: Changing El Niño–Southern Oscillation in a warming climate, *Nat. Rev.-Earth Environ.*, 2, 628–644,
657 <https://doi.org/10.1038/s43017-021-00199-z>, 2021.
- 658 Chen, S. F., Wu, R. G., and Chen, W.: Strengthened Connection between Springtime North Atlantic Oscillation and
659 North Atlantic Tripole SST Pattern since the Late 1980s, *J. Climate*, 35, 2007–2022,
660 <https://doi.org/10.1175/JCLI-D-19-0628.1>, 2020.
- 661 Chen, S. F., Chen W., Xie, S. P., Yu, B., Wu, R. G., Wang, Z. B., Lan, X. Q., and Graf, H.: Strengthened impact of
662 boreal winter North Pacific Oscillation on ENSO development in warming climate, *npj Climate and*
663 *Atmospheric Science*, 7, 69, <https://doi.org/10.1038/s41612-024-00615-3>, 2024.
- 664 Chen, S.Y., Zhao, D., Huang, J. P., He, J. Q., Chen, Y., Chen, J. Y., Bi, H. R., Lou, G. T., Du, S. K., Zhang, Y., and
665 Yang, F.: Mongolia Contributed More than 42% of the Dust Concentrations in Northern China in March and
666 April 2023, *Adv. Atmos. Sci.*, 40, 1549–1557, <https://doi.org/10.1007/s00376-023-3062-1>, 2023.
- 667 Csavina, J., Field, J., Félix, O., Corral-Avitia, A. Y., Sáez, A. E., and Betterton, E. A.: Effect of wind speed and
668 relative humidity on atmospheric dust concentrations in semi-arid climates, *Sci. Total Environ.*, 487, 82–90,
669 <https://doi.org/10.1016/j.scitotenv.2014.03.138>, 2014.
- 670 Ding, R. Q., Nnamchi, H. C., Yu, J. Y., Li, T., Sun, C., Li, J. P., Tseng, Y., Li, X. C., Xie, F., Feng, J., Ji, K., and Li,
671 X. M.: North Atlantic oscillation controls multidecadal changes in the North Tropical Atlantic–Pacific
672 connection, *Nat. Commun.*, 14, 862, <https://doi.org/10.1038/s41467-023-36564-3>, 2023.
- 673 Fan, K., Xie, Z. M., Wang, H. J., Xu, Z. Q., and Liu, J. P.: Frequency of spring dust weather in North China linked
674 to sea ice variability in the Barents Sea, *Clim. Dyn.*, 51, 4439–4450, [https://doi.org/10.1007/s00382-016-3515-](https://doi.org/10.1007/s00382-016-3515-7)
675 7, 2018.
- 676 Feldstein, S. B.: The dynamics of NAO teleconnection pattern growth and decay, *Q. J. Roy. Meteor. Soc.*, 129, 901–
677 924, <https://doi.org/10.1256/qj.02.76>, 2003.
- 678 Feng, J. and Li, J. P.: Influence of El Niño Modoki on spring rainfall over south China, *J. Geophys. Res.-Atmos.*,
679 116, D13102, <https://doi.org/10.1029/2010JD015160>, 2011.
- 680 Feng, J., Li, J. P., Liao, H., and Zhu, J. L.: Simulated coordinated impacts of the previous autumn North Atlantic
681 Oscillation (NAO) and winter El Niño on winter aerosol concentrations over eastern China, *Atmos. Chem.*
682 *Phys.*, 19, 10787–10800, <https://doi.org/10.5194/acp-19-10787-2019>, 2019.
- 683 Feng, J., Wang, S., and Li, J. P.: Strengthened ENSO amplitude contributed to regime shift in the Hadley circulation.
684 *Geophys. Res. Lett.*, 51, e2023GL106006. <https://doi.org/10.1029/2023GL106006>, 2024.

685 Feng, J., Zhu, J. L., Li, J. P., and Liao, H.: Aerosol concentrations variability over China: two distinct leading modes,
686 *Atmos. Chem. Phys.*, 20, 9883–9893, <https://doi.org/10.5194/acp-20-9883-2020>, 2020.

687 Gelaro, R., McCarty, W., Suárez, M. J., Todling, R., Molod, A., Takacs, L., Randles, C. A., Darmenov, A., Bosilovich,
688 M. G., Reichle, R., Wargan, K., Coy, L., Cullather, R., Draper, C., Akella, S., Buchard, V., Conaty, A., Da Silva,
689 A. M., Gu, W., Kim, G.-K., Koster, R., Lucchesi, R., Merkova, D., Nielsen, J. E., Partyka, G., Pawson, S.,
690 Putman, W., Rienecker, M., Schubert, S. D., Sienkiewicz, M., and Zhao, B.: The Modern-Era Retrospective
691 Analysis for Research and Applications, Version 2 (MERRA-2), *J. Climate*, 30, 5419–5454,
692 <https://doi.org/10.1175/JCLI-D-16-0758.1>, 2017.

693 Gong, S. L., Zhang, X. Y., Zhao, T. L., Zhang, X. B., Barrie, L. A., McKendry, I. G., and Zhao, C. S.: A Simulated
694 Climatology of Asian Dust Aerosol and Its Trans-Pacific Transport. Part II: Interannual Variability and Climate
695 Connections, *J. Climate*, 19, 104–122, <https://doi.org/10.1175/JCLI3606.1>, 2006.

696 Guo, Y., Li, J. P., and Li, Y.: A Time-Scale Decomposition Approach to Statistically Downscale Summer Rainfall
697 over North China, *J. Climate*, 25, 572–591, <https://doi.org/10.1175/JCLI-D-11-00014.1>, 2012.

698 Hersbach, H., Bell, B., Berrisford, P., Hirahara, S., Horányi, A., Muñoz-Sabater, J., Nicolas, J., Peubey, C., Radu, R.,
699 Schepers, D., Simmons, A., Soci, C., Abdalla, S., Abellan, X., Balsamo, G., Bechtold, P., Biavati, G., Bidlot, J.,
700 Bonavita, M., De Chiara, G., Dahlgren, P., Dee, D., Diamantakis, M., Dragani, R., Flemming, J., Forbes, R.,
701 Fuentes, M., Geer, A., Haimberger, L., Healy, S., Hogan, R. J., Hólm, E., Janisková, M., Keeley, S., Laloyaux,
702 P., Lopez, P., Lupu, C., Radnoti, G., De Rosnay, P., Rozum, I., Vamborg, F., Villaume, S., and Thépaut, J.: The
703 ERA5 global reanalysis, *Q. J. Roy. Meteor. Soc.*, 146, 1999–2049, <https://doi.org/10.1002/qj.3803>, 2020.

704 Hu, Z. Y., Ma, Y. Y., Jin, Q. J., Idrissa, N. F., Huang, J. P., and Dong, W. J.: Attribution of the March 2021 exceptional
705 dust storm in North China, *B. Am. Meteorol. Soc.*, 104, E749–E755, [https://doi.org/10.1175/BAMS-D-22-](https://doi.org/10.1175/BAMS-D-22-0151.1)
706 [0151.1](https://doi.org/10.1175/BAMS-D-22-0151.1), 2023.

707 Huang, J., Li, Y., Fu, C., Chen, F., Fu, Q., Dai, A., Shinoda, M., Ma, Z., Guo, W., Li, Z., Zhang, L., Liu, Y., Yu, H.,
708 He, Y., Xie, Y., Guan, X., Ji, M., Lin, L., Wang, S., Yan, H., and Wang, G.: Dryland climate change: Recent
709 progress and challenges, *Rev. Geophys.*, 55, 719–778, <https://doi.org/10.1002/2016RG000550>, 2017.

710 Huang, J. P., Liu, J. J., Chen, B., and Nasiri, S. L.: Detection of anthropogenic dust using CALIPSO lidar
711 measurements, *Atmos. Chem. Phys.*, 15, 11653–11665, <https://doi.org/10.5194/acp-15-11653-2015>, 2015.

712 Huang, Y. H., Liu, X. D., Yin, Z., and An, Z. S.: Global Impact of ENSO on Dust Activities with Emphasis on the
713 Key Region from the Arabian Peninsula to Central Asia, *J. Geophys. Res.-Atmos.*, 126, e2020JD034068,
714 <https://doi.org/10.1029/2020JD034068>, 2021.

715 Hurrell, J. W.: Decadal Trends in the North Atlantic Oscillation: Regional Temperatures and Precipitation, *Science*,
716 269, 676–679, <https://doi.org/10.1126/science.269.5224.676>, 1995.

717 Ji, L. Q. and Fan, K.: Climate prediction of dust weather frequency over northern China based on sea-ice cover and
718 vegetation variability, *Clim. Dyn.*, 53, 687–705, <https://doi.org/10.1007/s00382-018-04608-w>, 2019.

719 Jia, X. J., Derome, J., and Lin, H.: Comparison of the Life Cycles of the NAO Using Different Definitions, *J. Climate*,
720 20, 5992–6011, <https://doi.org/10.1175/2007JCLI1408.1>, 2007.

721 Jiang, W. P., Huang, G., Huang, P., Wu, R. G., Hu, K. M., and Chen, W.: Northwest Pacific Anticyclonic Anomalies
722 during Post–El Niño Summers Determined by the Pace of El Niño Decay, *J. Climate*, 32, 3487–3503,
723 <https://doi.org/10.1175/JCLI-D-18-0793.1>, 2019.

724 Jiménez-Esteve, B. and Domeisen, D. I. V.: The Tropospheric Pathway of the ENSO–North Atlantic Teleconnection,
725 *J. Climate*, 31, 4563–4584, <https://doi.org/10.1175/JCLI-D-17-0716.1>, 2018.

726 Jones, P. D., Jonsson, T., and Wheeler, D.: Extension to the North Atlantic Oscillation using early instrumental
727 pressure observations from Gibraltar and South-West Iceland. *Int. J. Climatol.*, 17, 1433–1450,
728 [https://doi.org/10.1002/\(SICI\)1097-0088\(19971115\)17:13<1433::AID-JOC203>3.0.CO;2-P](https://doi.org/10.1002/(SICI)1097-0088(19971115)17:13<1433::AID-JOC203>3.0.CO;2-P), 1997.

729 Kang, L. T., Huang, J. P., Chen, S. Y., and Wang, X.: Long-term trends of dust events over Tibetan Plateau during
730 1961-2010, *Atmos. Environ.*, 125, 188-198, <https://doi.org/10.1016/j.atmosenv.2015.10.085>, 2016.

731 Ke, M. L., Wang, Z. Q., Pan, W. J., Luo, H. L., Yang, S., and Guo, R. Y.: Extremely Strong Western Pacific
732 Subtropical High in May 2021 Following a La Niña Event: Role of the Persistent Convective Forcing over the
733 Indian Ocean, *Asia-pac. J. Atmos. Sci.*, 59, 47–58, <https://doi.org/10.1007/s13143-022-00300-6>, 2023.

734 Kim, H. and Choi, M.: Impact of soil moisture on dust outbreaks in East Asia: Using satellite and assimilation data,
735 *Geophys. Res. Lett.*, 42, 2789–2796, <https://doi.org/10.1002/2015GL063325>, 2015.

736 Kim, S. and Kug, J.: What Controls ENSO Teleconnection to East Asia? Role of Western North Pacific Precipitation
737 in ENSO Teleconnection to East Asia, *J. Geophys. Res.-Atmos.*, 123, <https://doi.org/10.1029/2018JD028935>,
738 2018.

739 Kok, J. F., Storelvmo, T., Karydis, V. A., Adebisi, A. A., Mahowald, N. M., Evan, A. T., He, C. L., and Leung, D.
740 M.: Mineral dust aerosol impacts on global climate and climate change, *Nat. Rev.-Earth Environ.*, 4, 71–86,
741 <https://doi.org/10.1038/s43017-022-00379-5>, 2023.

742 Li, J. P., and Wang, J. X. L.: A new North Atlantic Oscillation index and its variability, *Adv. Atmos. Sci.*, 20, 661–
743 676, <https://doi.org/10.1007/BF02915394>, 2003.

744 Li, J. P., Zheng, F., Sun, C., Feng, J., and Wang, J.: Pathways of Influence of the Northern Hemisphere Mid-high
745 Latitudes on East Asian Climate: A Review, *Adv. Atmos. Sci.*, 36, 902–921, <https://doi.org/10.1007/s00376-019-8236-5>, 2019.

747 Li, J., Carlson, B. E., Yung, Y. L., Lv, D., Hansen, J., Penner, J. E., Liao, H., Ramaswamy, V., Kahn, R. A., Zhang,
748 P., Dubovik, O., Ding, A. J., Lacis, A. A., Zhang, L., and Dong, Y. M.: Scattering and absorbing aerosols in the
749 climate system, *Nat. Rev.-Earth Environ.*, 3, 363–379, <https://doi.org/10.1038/s43017-022-00296-7>, 2022.

750 Li, Y., Xu, F. L., Feng, J., Du, M. Y., Song, W. J., Li, C., and Zhao, W. J.: Influence of the previous North Atlantic
751 Oscillation (NAO) on the spring dust aerosols over North China, *Atmos. Chem. Phys.*, 23, 6021–6042,
752 <https://doi.org/10.5194/acp-23-6021-2023>, 2023.

753 Liu, X. D., Yin, Z., Zhang, X. Y., and Yang, X. C.: Analyses of the spring dust storm frequency of northern China in
754 relation to antecedent and concurrent wind, precipitation, vegetation, and soil moisture conditions, *J. Geophys.*
755 *Res.-Atmos.*, 109, 2004JD004615, <https://doi.org/10.1029/2004JD004615>, 2004.

756 López-Parages, J., Rodríguez-Fonseca, B., and Terray, L.: A mechanism for the multidecadal modulation of ENSO
757 teleconnection with Europe, *Clim. Dyn.*, 45, 867–880, <https://doi.org/10.1007/s00382-014-2319-x>, 2015.

758 Lou, S. J., Russell, L. M., Yang, Y., Xu, L., Lamjiri, M. A., DeFlorio, M. J., Miller, A. J., Ghan, S. J., Liu, Y., and
759 Singh, B.: Impacts of the East Asian Monsoon on springtime dust concentrations over China, *J. Geophys. Res.-*
760 *Atmos.*, 121, 8137–8152, <https://doi.org/10.1002/2016JD024758>, 2016.

761 Lou, S. J., Russell, L. M., Yang, Y., Liu, Y., Singh, B., and Ghan, S. J.: Impacts of interactive dust and its direct
762 radiative forcing on interannual variations of temperature and precipitation in winter over East Asia, *J. Geophys.*
763 *Res.-Atmos.*, 122, 8761–8780, <https://doi.org/10.1002/2017JD027267>, 2017.

764 McPhaden, M. J. and Zhang, X. B.: Asymmetry in zonal phase propagation of ENSO sea surface temperature
765 anomalies, *Geophys. Res. Lett.*, 36, 2009GL038774, <https://doi.org/10.1029/2009GL038774>, 2009.

766 Najibi, N., Devineni, N., and Lall, U.: Compound Continental Risk of Multiple Extreme Floods in the United States.
767 *Geophys. Res. Lett.*, 50, e2023GL105297. <https://doi.org/10.1029/2023GL105297>, 2023.

768 Pan, L. L.: Observed positive feedback between the NAO and the North Atlantic SSTA tripole, *Geophys. Res. Lett.*,
769 32, 2005GL022427, <https://doi.org/10.1029/2005GL022427>, 2005.

770 Parry, S., Lavers, D., Wilby, R., Prudhomme, C., Wood, P., Murphy, C., and O'Connor, P.: Abrupt drought termination
771 in the British–Irish Isles driven by high atmospheric vapour transport, *Environ. Res. Lett.*, 18, 104050,
772 <https://doi.org/10.1088/1748-9326/acf145>, 2023.

773 Prospero, J. M., Nees, R. T., and Uematsu, M.: Deposition rate of particulate and dissolved aluminum derived from
774 saharan dust in precipitation at Miami, Florida, *J. Geophys. Res.-Atmos.*, 92, 14723–14731,
775 <https://doi.org/10.1029/JD092iD12p14723>, 1987.

776 Rayner, N. A., Parker, D. E., Horton, E. B., Folland, C. K., Alexander, L. V., Rowell, D. P., Kent, E. C., and Kaplan,
777 A.: Global analyses of sea surface temperature, sea ice, and night marine air temperature since the late
778 nineteenth century, *J. Geophys. Res.-Atmos.*, 108, 2002JD002670, <https://doi.org/10.1029/2002JD002670>,
779 2003.

780 Song, L. Y., Chen, S. F., Chen, W., Guo, J. P., Cheng, C. L., and Wang, Y.: Distinct evolutions of haze pollution from
781 winter to following spring over the North China Plain: Role of the North Atlantic sea surface temperature
782 anomalies. *Atmos. Chem. Phys.*, 22, 1669–1688, <https://doi.org/10.5194/acp-22-1669-2022>, 2022.

783 Su, J. Z., Zhang, R. H., Li, T., Rong, X. Y., Kug, J., and Hong, C.: Causes of the El Niño and La Niña Amplitude
784 Asymmetry in the Equatorial Eastern Pacific, *J. Climate*, 23, 605–617, <https://doi.org/10.1175/2009JCLI2894.1>,
785 2010.

786 Sung, M., Lim, G., and Kug, J.: Phase asymmetric downstream development of the North Atlantic Oscillation and
787 its impact on the East Asian winter monsoon, *J. Geophys. Res.-Atmos.*, 115, 2009JD013153,
788 <https://doi.org/10.1029/2009JD013153>, 2010.

789 Takaya, K. and Nakamura, H.: A Formulation of a Phase-Independent Wave-Activity Flux for Stationary and
790 Migratory Quasigeostrophic Eddies on a Zonally Varying Basic Flow, *J. Atmospheric Sci.*, 58, 608–627,
791 [https://doi.org/10.1175/1520-0469\(2001\)058<0608:AFOAPI>2.0.CO;2](https://doi.org/10.1175/1520-0469(2001)058<0608:AFOAPI>2.0.CO;2), 2001.

792 Trenberth, K. E.: The Definition of El Niño, *B. Am. Meteorol. Soc.*, 78, 2771–2777, [https://doi.org/10.1175/1520-0477\(1997\)078<2771:TDOENO>2.0.CO;2](https://doi.org/10.1175/1520-0477(1997)078<2771:TDOENO>2.0.CO;2), 1997.

794 Wallace, J. M. and Gutzler, D. S.: Teleconnections in the Geopotential Height Field during the Northern Hemisphere
795 Winter, *Mon. Weather Rev.*, 109, 784–812, [https://doi.org/10.1175/1520-0493\(1981\)109<0784:TITGHF>2.0.CO;2](https://doi.org/10.1175/1520-0493(1981)109<0784:TITGHF>2.0.CO;2), 1981.

797 Wang, B., Wu, R. G., and Fu, X. H.: Pacific–East Asian Teleconnection: How Does ENSO Affect East Asian
798 Climate?, *J. Climate*, 13, 1517–1536, [https://doi.org/10.1175/1520-0442\(2000\)013<1517:PEATHD>2.0.CO;2](https://doi.org/10.1175/1520-0442(2000)013<1517:PEATHD>2.0.CO;2),
799 2000.

800 Wang, C., Ren, B. H., Li, G., Zheng, J. Q., Jiang, L. W., and Xu, D.: An Interdecadal Change in the Influence of the
801 NAO on Atlantic-Induced Arctic Daily Warming around the Mid-1980s, *Adv. Atmos. Sci.*, 40, 1285–1297,
802 <https://doi.org/10.1007/s00376-022-2218-8>, 2023.

803 Wang, L., and Ting, M. F.: Stratosphere-Troposphere Coupling Leading to Extended Seasonal Predictability of
804 Summer North Atlantic Oscillation and Boreal Climate, *Geophys. Res. Lett.*, 49, e2021GL096362.
805 <https://doi.org/10.1029/2021GL096362>, 2022.

806 Wang, T. H., Tang, J. Y., Sun, M. X., Liu, X. W., Huang, Y. X., Huang, J. P., Han, Y., Cheng, Y. F., Huang, Z. W., and
807 Li, J. M.: Identifying a transport mechanism of dust aerosols over South Asia to the Tibetan Plateau: A case
808 study, *Sci. Total Environ.*, 758, 11, <https://doi.org/10.1016/j.scitotenv.2020.143714>, 2021.

809 Wang, Z. Q., Yang, S., Lau, N.-C., and Duan, A. M.: Teleconnection between Summer NAO and East China Rainfall
810 Variations: A Bridge Effect of the Tibetan Plateau, *J. Climate*, 31, 6433–6444, <https://doi.org/10.1175/JCLI-D-17-0413.1>, 2018.

812 Woollings, T., Franzke, C., Hodson, D. L. R., Dong, B., Barnes, E. A., Raible, C. C., and Pinto, J. G.: Contrasting
813 interannual and multidecadal NAO variability, *Clim. Dyn.*, 45, 539–556, <https://doi.org/10.1007/s00382-014-2237-y>, 2015.

814

815 Wu, B., Zhou, T. J., and Li, T.: Atmospheric Dynamic and Thermodynamic Processes Driving the Western North
816 Pacific Anomalous Anticyclone during El Niño. Part I: Maintenance Mechanisms, *J. Climate*, 30, 9621–9635,
817 <https://doi.org/10.1175/JCLI-D-16-0489.1>, 2017.

818 Wu, J., Kurosaki, Y., Shinoda, M., and Kai, K.: Regional Characteristics of Recent Dust Occurrence and Its
819 Controlling Factors in East Asia, *Sola*, 12, 187–191, <https://doi.org/10.2151/sola.2016-038>, 2016.

820 Wu, R. G. and Chen, S. F.: What Leads to Persisting Surface Air Temperature Anomalies from Winter to Following
821 Spring over Mid- to High-Latitude Eurasia? *J. Climate*, 33, 5861–5883, <https://doi.org/10.1175/JCLI-D-19-0819.1>, 2020.

822

823 Wu, Z. W., Wang, B., Li, J. P., and Jin, F. F.: An empirical seasonal prediction model of the east Asian summer
824 monsoon using ENSO and NAO, *J. Geophys. Res.-Atmos.*, 114, 2009JD011733,
825 <https://doi.org/10.1029/2009JD011733>, 2009.

826 Wu, Z. W., Li, J. P., Jiang, Z. H., He, J. H., and Zhu, X. Y.: Possible effects of the North Atlantic Oscillation on the
827 strengthening relationship between the East Asian Summer monsoon and ENSO, *Int. J. Climatol.*, 32, 794–800,
828 <https://doi.org/10.1002/joc.2309>, 2012.

829 Xi, X. and Sokolik, I. N.: Dust interannual variability and trend in Central Asia from 2000 to 2014 and their climatic
830 linkages, *J. Geophys. Res.-Atmos.*, 120, <https://doi.org/10.1002/2015JD024092>, 2015.

831 Yang, Y., Zeng, L. Y., Wang, H. L., Wang, P. Y., and Liao, H.: Dust pollution in China affected by different spatial
832 and temporal types of El Niño, *Atmos. Chem. Phys.*, 22, 14489–14502, <https://doi.org/10.5194/acp-22-14489-2022>, 2022.

833

834 Yao, W. R., Gui, K., Wang, Y. Q., Che, H. Z., and Zhang, X. Y.: Identifying the dominant local factors of 2000–2019
835 changes in dust loading over East Asia, *Sci. Total Environ.*, 777, 146064,
836 <https://doi.org/10.1016/j.scitotenv.2021.146064>, 2021.

837 Yu, Y., Notaro, M., Liu, Z. Y., Wang, F. Y., Alkolibi, F., Fadda, E., and Bakhrjy, F.: Climatic controls on the
838 interannual to decadal variability in Saudi Arabian dust activity: Toward the development of a seasonal dust
839 prediction model, *J. Geophys. Res.-Atmos.*, 120, 1739–1758, <https://doi.org/10.1002/2014JD022611>, 2015.

840 Zhang, P., Wu, Z. W., and Jin, R.: How can the winter North Atlantic Oscillation influence the early summer
841 precipitation in Northeast Asia: effect of the Arctic sea ice, *Clim. Dyn.*, 56, 1989–2005,
842 <https://doi.org/10.1007/s00382-020-05570-2>, 2021a.

843 Zhang, R. H., Li, T. R., Wen, M., and Liu, L. K.: Role of intraseasonal oscillation in asymmetric impacts of El Niño
844 and La Niña on the rainfall over southern China in boreal winter, *Clim. Dyn.*, 45, 559–567,
845 <https://doi.org/10.1007/s00382-014-2207-4>, 2015.

846 Zhang, R. H., Tian, W. S., He, X., Qie, K., Liu, D., and Tian, H. Y.: Enhanced influence of ENSO on winter
847 precipitation over southern China in recent decades, *J. Climate*, 1–36, <https://doi.org/10.1175/JCLI-D-21-0182.1>, 2021b.

848

849 Zhang, W. J., Li, J. P., and Jin, F. F.: Spatial and temporal features of ENSO meridional scales, *Geophys. Res. Lett.*,
850 36, 2009GL038672, <https://doi.org/10.1029/2009GL038672>, 2009.

851 Zhang, W. J., Li, H. Y., Stuecker, M. F., Jin, F. F., and Turner, A. G.: A New Understanding of El Niño’s Impact over
852 East Asia: Dominance of the ENSO Combination Mode, *J. Climate*, 29, 4347–4359,
853 <https://doi.org/10.1175/JCLI-D-15-0104.1>, 2016.

854 Zhang, X. Y., Gong, S. L., Zhao, T. L., Arimoto, R., Wang, Y. Q., and Zhou, Z. J.: Sources of Asian dust and role of
855 climate change versus desertification in Asian dust emission, *Geophys. Res. Lett.*, 30, 2003GL018206,
856 <https://doi.org/10.1029/2003GL018206>, 2003.

857 Zhao, C. F., Yang, Y. K., Fan, H., Huang, J. P., Fu, Y. F., Zhang, X. Y., Kang, S. C., Cong, Z. Y., Letu, H., and Menenti,
858 M.: Aerosol characteristics and impacts on weather and climate over the Tibetan Plateau, *Natl. Sci. Rev.*, 7,
859 492–495, <https://doi.org/10.1093/nsr/nwz184>, 2020.

860 Zhao, S., Li, J. P., and Sun, C.: Decadal variability in the occurrence of wintertime haze in central eastern China tied
861 to the Pacific Decadal Oscillation, *Sci. Rep.*, 6, 27424, <https://doi.org/10.1038/srep27424>, 2016.

862 Zhao, Y., Huang, A. N., Zhu, X. S., Zhou, Y., and Huang, Y.: The impact of the winter North Atlantic Oscillation on
863 the frequency of spring dust storms over Tarim Basin in northwest China in the past half-century, *Environ. Res.
864 Lett.*, 8, 024026, <https://doi.org/10.1088/1748-9326/8/2/024026>, 2013.

865 Zheng, F., Li, J. P., Li, Y. J., Zhao, S., and Deng, D. F.: Influence of the Summer NAO on the Spring-NAO-Based
866 Predictability of the East Asian Summer Monsoon, *J. Appl. Meteorol. Clim.*, 55, 1459–1476,
867 <https://doi.org/10.1175/JAMC-D-15-0199.1>, 2016a.

868 Zheng, Y., Zhao, T. L., Che, H. Z., Liu, Y., Han, Y. X., Liu, C., Xiong, J., Liu, J. H., and Zhou, Y. K.: A 20-year
869 simulated climatology of global dust aerosol deposition, *Sci. Total Environ.*, 557–558, 861–868,
870 <https://doi.org/10.1016/j.scitotenv.2016.03.086>, 2016b.

871 Zhou, F., Shi, J., Liu, M. H., and Ren, H. C.: Linkage between the NAO and Siberian high events on the intraseasonal
872 timescale, *Atmos. Res.*, 281, 106478, <https://doi.org/10.1016/j.atmosres.2022.106478>, 2023.

873 Zhu, C. W., Wang, B., and Qian, W. H.: Why do dust storms decrease in northern China concurrently with the recent
874 global warming? *Geophys. Res. Lett.*, 35, 2008GL034886, <https://doi.org/10.1029/2008GL034886>, 2008.

875 Zuo, J. Q., Ren, H. L., Li, W. J., and Wang, L.: Interdecadal Variations in the Relationship between the Winter North
876 Atlantic Oscillation and Temperature in South-Central China, *J. Climate*, 29, 7477–7493,
877 <https://doi.org/10.1175/JCLI-D-15-0873.1>, 2016.